Article

Current Biology

Functional and ultrastructural analysis of reafferent mechanosensation in larval zebrafish

Highlights

- Lateral line sensory neurons are insensitive to reafferent flow during locomotion
- Cholinergic efferent neurons suppress reafferent stimulation
- Nicotinic acetylcholine receptors containing α9 subunits mediate this inhibition
- Dopaminergic efferents are activated during locomotion and by sensory stimuli

Authors

Iris Odstrcil, Mariela D. Petkova, Martin Haesemeyer, ..., Ruben Portugues, Jeff W. Lichtman, Florian Engert

Correspondence

iris.odstrcil@protonmail.com (I.O.), florian@mcb.harvard.edu (F.E.)

In brief

Odstrcil et al. show that cholinergic efferents inhibit hair cells of the lateral line during locomotion, thereby cancelling self-generated stimulation when zebrafish larvae are moving. Inhibition depends on α9 nicotinic-receptor subunits. Dopaminergic efferents are activated by sensory stimuli and during locomotion, but their role remains elusive.

Odstrcil et al., 2022, Current Biology *32*, 1–14
January 10, 2022
https://doi.org/10.1016/j.cub.2021.11.007

CellPress

Please cite this article in press as: Odstrcil et al., Functional and ultrastructural analysis of reafferent mechanosensation in larval zebrafish, Current Biology (2021), https://doi.org/10.1016/j.cub.2021.11.007

Current Biology

CellPress
OPEN ACCESS

Article

Functional and ultrastructural analysis of reafferent mechanosensation in larval zebrafish

Iris Odstrcil,[1,2,11,13,*] Mariela D. Petkova,[1,2] Martin Haesemeyer,[3] Jonathan Boulanger-Weill,[1,2] Maxim Nikitchenko,[4] James A. Gagnon,[5,6] Pablo Oteiza,[7] Richard Schalek,[1,2] Adi Peleg,[1] Ruben Portugues,[8,9,10] Jeff W. Lichtman,[1,2,12] and Florian Engert[1,2,12,14,15,*]

[1]Department of Molecular and Cellular Biology, Faculty of Arts and Sciences, Harvard University, Cambridge, MA 02138, USA
[2]Center for Brain Science, Faculty of Arts and Sciences, Harvard University, Cambridge, MA 02138, USA
[3]The Ohio State University, Department of Neuroscience, Columbus, OH 43210, USA
[4]Duke University School of Medicine, Durham, NC 27707, USA
[5]School of Biological Sciences, University of Utah, Salt Lake City, UT 84112, USA
[6]Center for Cell & Genome Science, University of Utah, Salt Lake City, UT 84112, USA
[7]Max Planck Institute for Ornithology, Flow Sensing Research Group, Seewiesen 82319, Germany
[8]Institute of Neuroscience, Technical University of Munich, Munich 80333, Germany
[9]Max Planck Institute of Neurobiology, Research Group of Sensorimotor Control, Martinsried 82152, Germany
[10]Munich Cluster for Systems Neurology (SyNergy), Munich 81377, Germany
[11]Present address: Friedrich Miescher Institute for Biomedical Research, Basel 4058, Switzerland
[12]These authors contributed equally
[13]Twitter: @IrisOdstrcil
[14]Twitter: @EngertLab
[15]Lead contact
*Correspondence: iris.odstrcil@protonmail.com (I.O.), florian@mcb.harvard.edu (F.E.)
https://doi.org/10.1016/j.cub.2021.11.007

SUMMARY

All animals need to differentiate between exafferent stimuli, which are caused by the environment, and reafferent stimuli, which are caused by their own movement. In the case of mechanosensation in aquatic animals, the exafferent inputs are water vibrations in the animal's proximity, which need to be distinguishable from the reafferent inputs arising from fluid drag due to locomotion. Both of these inputs are detected by the lateral line, a collection of mechanosensory organs distributed along the surface of the body. In this study, we characterize in detail how hair cells—the receptor cells of the lateral line—in zebrafish larvae discriminate between such reafferent and exafferent signals. Using dye labeling of the lateral line nerve, we visualize two parallel descending inputs that can influence lateral line sensitivity. We combine functional imaging with ultra-structural EM circuit reconstruction to show that cholinergic signals originating from the hindbrain transmit efference copies (copies of the motor command that cancel out self-generated reafferent stimulation during locomotion) and that dopaminergic signals from the hypothalamus may have a role in threshold modulation, both in response to locomotion and salient stimuli. We further gain direct mechanistic insight into the core components of this circuit by loss-of-function perturbations using targeted ablations and gene knockouts. We propose that this simple circuit is the core implementation of mechanosensory reafferent suppression in these young animals and that it might form the first instantiation of state-dependent modulation found at later stages in development.

INTRODUCTION

To respond appropriately to their environment, animals must distinguish between exafferent sensory inputs caused by external sources and reafferent signals generated by their own motion. Solutions to this informational ambiguity involve completely blocking sensory pathways during locomotion or precisely subtracting reafferent inputs to isolate exafferent signals. An early observation of this phenomenon was made by von Helmholtz, who noted that visual information must be transiently suppressed during eye saccades since our ability to process visual images is severely compromised during these movements.[1] Since then, complete sensory suppression or reafferent cancellation has been observed across modalities and species throughout the animal kingdom (see reviews[2–4]). Examples include the suppression of reafferent sounds in zebra finches and mice,[5–7] suppression of reafferent somatosensation during crayfish escapes or fish respiratory and fin movements,[8,9] and the subtraction of visual flow during body saccades in *Drosophila*.[10] At their core, all these implementations rely on corollary discharges or efference copies: signals from motor-command centers that inform the sensory processing pathway about impending movements.[11,12]

One of the first dissections of the neural mechanisms underlying reafferent cancellation was accomplished in weakly electric fish. These animals emit electrical discharges and detect the

Please cite this article in press as: Odstrcil et al., Functional and ultrastructural analysis of reafferent mechanosensation in larval zebrafish, Current Biology (2021), https://doi.org/10.1016/j.cub.2021.11.007

distortions in the resulting field lines using electrosensory receptor organs in the lateral line. Notably, the self-generated electrical pulses themselves are adaptively cancelled out by cerebellar-like structures precisely tuned to subtract a copy of the expected incoming sensory information in a flexible and dynamic fashion.[13–15]

Most fish and amphibians lack electrosensory organs and use the lateral line exclusively to sense water motion relative to their bodies.[16] This information is important for numerous behaviors such as schooling,[17] prey capture,[18] predator avoidance,[19] and rheotaxis.[20,21] Because fluid drag during locomotion strongly activates the lateral line,[22] in this case too, external and self-generated stimuli must be processed differentially. Indeed, the transient inhibition of the afferent lateral nerve during locomotor events has been observed in tadpoles[23,24] and diverse fish species,[25,26] including zebrafish.[27,28] While the general characteristics of this phenomenon appear to be maintained, the specific details regarding connectivity, anatomy, and function can vary across species (see Coombs et al.[29] for a comprehensive review).

Specifically in the zebrafish, two efferent pathways targeting the lateral line have been identified: the cholinergic octavolateral efferent nucleus (OEN) in the hindbrain and the dopaminergic efferent to the lateral line (DELL) in the ventral hypothalamus.[30,31] Further, acetylcholine has been shown to inhibit hair cell activity,[32,33] making the OEN the most likely source of reafferent suppression. At the synaptic level, ideas about how acetylcholine may inhibit hair cells come from studies on efferent innervation of the auditory and vestibular systems.[34] In the rat cochlea, the hyperpolarizing effects of acetylcholine result from the activation of nicotinic receptors containing $\alpha9/\alpha10$ subunits.[35,36] This inhibitory effect, however, is less related to reafferent suppression and is thought to have a protective function against excitotoxicity during acoustic hyperstimulation.[6,7,37] In lateral line hair cells of larval zebrafish, enriched expression of the $\alpha9$, but not the $\alpha10$, subunits has been observed.[32,38] Whether this plays a role in protective silencing, context-dependent modulation, or reafferent suppression has not yet been determined. Nonetheless, there is now significant evidence for the role of cholinergic efferents in reafferent suppression, and their mechanism has been hypothesized to the level of individual receptor subtypes. The functional role and mechanism of the dopaminergic efferent neurons, on the other hand, is still unclear.

It is further unknown how all the cell populations, namely, the two efferent subtypes (OEN and DELL) as well as the afferent sensory neurons and the hair cells of the neuromasts, are interconnected and give rise to a microcircuit that can adaptively process the sensory signals detected by the lateral line.

In this study, we exploit the small size and optical accessibility of the young (7 days-post-fertilization [dpf]) zebrafish larvae, which afford a unique opportunity to perform an exhaustive anatomical and functional dissection of the microcircuitry surrounding the neuromasts of the lateral line. To that end, we first described the identity and morphology of descending inputs to the lateral line. We then used a combination of confocal and electron microscopy (EM) to unveil the detailed synaptic structures between efferent terminals, afferent neurites, and the hair cells of the neuromast. Using functional imaging during behavior, we detected activation of both OEN and DELL neurons during locomotion and a concomitant absence of afferent activity. However, targeted laser ablation of individual efferent populations established that OEN, but not DELL, neurons are necessary for the suppression of reafferent activity. We further confirmed the critical role of the cholinergic pathway and established the necessity of the $\alpha9$ cholinergic subunit in hair cells by means of gene knockout approaches. Additionally, we observed that DELL, but not OEN, neurons respond to flow, acoustic, and visual stimuli in the absence of motor outputs—unveiling a sensory capacity in these dopaminergic neurons that could be used to modulate mechanosensation in response to environmental cues.

Taken together, our results identify the OEN as the source of efference copy signaling to the lateral line and allow us to propose the hypothesis that DELL neurons serve to modulate hair cell sensitivity during the quiescent periods following locomotion and after the occurrence of salient stimuli.

RESULTS

Anatomy

If efference copy mechanisms are in place to cancel out self-generated mechanosensory stimulation during locomotion, there must exist an anatomical bridge between the motor and the sensory streams of the lateral line. In zebrafish larvae, axons from the brain directly innervate the peripheral mechanosensory organs, the neuromasts[30] (Figure 1A). These axons reach the tail neuromasts via the posterior lateral line nerve (PLLn), a superficial nerve that also comprises the dendrites of primary sensory neurons (Figure 1B). As in previous studies, by injecting the PLLn with fluorescent dextrans, we could visualize all neuronal populations that target the tail neuromasts: the primary sensory neurons of the posterior lateral line ganglion (PLLg) and the two efferent nuclei, the DELL and the OEN (Figures 1C and 1D).[30,31] The OEN is further subdivided into rostral and caudal subnuclei, according to the relative positions of the soma of the cells that comprise them and the location at which their axons exit the brain (Figures 1D and S1A).[30] Dye labeling of multiple animals and subsequent image registration revealed that OEN neurons also occupy a third position in the hindbrain at the level of rhombomere 4 (Figure S1A), which we have termed the supra-rostral OEN (srOEN).

To further characterize the system, we sought to confirm the primary neurotransmitter identity of both nuclei by performing dextran injections in transgenic fish lines that label dopaminergic (DAT:GFP), mono-aminergic (ETvmat2:GFP), or largely cholinergic (Isl1:GFP) neurons. Since Isl1 is expressed by a variety of neurons, we supplemented these injections with immunohistochemical stains against choline acetyltransferase. In line with previous work, we observed that DELL neurons are dopaminergic and OEN neurons are cholinergic (Figures S1B and S1C).[39,40] Furthermore, we corroborated that the above-mentioned transgenic lines label the lateral-line efferent neurons and can be used as anatomical markers for subsequent experiments.

To understand the organization principles of this circuit, we performed single-cell focal electroporations to label individual neurons with membrane-tagged fluorescent proteins and analyzed their arborization patterns. We focused on neuronal morphology and asked whether efferent nuclei are

Please cite this article in press as: Odstrcil et al., Functional and ultrastructural analysis of reafferent mechanosensation in larval zebrafish, Current Biology (2021), https://doi.org/10.1016/j.cub.2021.11.007

CellPress
OPEN ACCESS

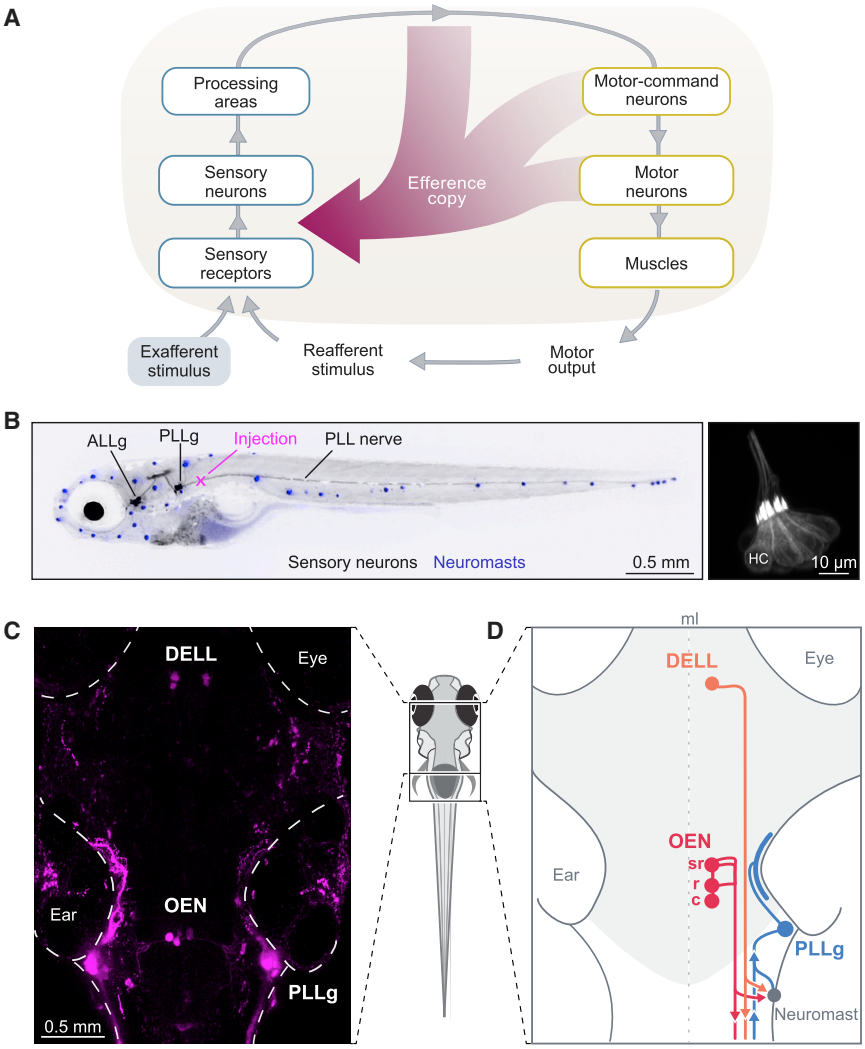

Figure 1. Efference copy signals and lateral line circuitry

(A) Schematic of a sensorimotor circuit comprising a sensory (blue) and motor pathway (yellow). Efference copy or corollary discharge signals (crimson) can arise from almost any level of the motor pathway and target any level in the sensory pathway. In the zebrafish, centrifugal fibers from the brain target the neuromasts directly. Adapted from Crapse and Sommer.[2]

(B) Left: lateral view of a 7 days-post-fertilization (dpf) larva expressing GFP in lateral line sensory neurons (black). Anterior lateral line ganglion (ALLg) neurons innervate head neuromasts, and posterior lateral line ganglion (PLLg) neurons innervate dorsal and tail neuromasts. Neuromasts with hair cells stained with DiASP (blue). Backfills of the posterior lateral line nerve (PLLn) via dye injections (magenta cross). Right: hair cells (HC) expressing GFP in a posterior neuromast of a 7 dpf larva.

(C) Maximum intensity projection of the brain of a 6 dpf larva that received bilateral injections of fluorescent dextrans in the PLLn. Labeling reveals 3 cell clusters: the PLLg, the DELL, and the OEN with its caudal, rostral, and supra-rostral subdivisions. In this fish, only the caudal OEN was labeled.

(D) Diagram showing the major components of the posterior lateral line circuit in the brain (light gray) and periphery. Neuromasts, sensory organs (gray), are activated by mechanosensory stimuli. Signals are transmitted to primary sensory/afferents neurons in the PLLg (light blue). Descending inputs originate from the DELL (orange) and from the OEN (red). Afferent and efferent neurites join in the PLLn and extend collateral branches to individual neuromasts. The circuit is midline (ml) symmetric, but only one side is illustrated for clarity.

See also Figure S1.

somatotopically organized—whether the position of a neuron's soma within the nucleus correlates with the rostro-caudal distribution of its recipient neuromasts. We found that neither the DELL nor OEN are strictly somatotopically organized (Figure S1E). Individual DELL neurons extend neurites ipsilaterally and innervate a wide range of targets: neuromasts of the head and tail, hair cells of the inner ear, and the spinal cord (Figures S1D [top] andS1E).[41–43] Individual OEN neurons possess bilateral dendritic arbors, and their axons project ipsilaterally to contact hair cells of the inner ear and anterior and posterior neuromasts (Figures S1D and S1E). We observed any combination of targets besides the inner ear alone (Figure S1E). Notably, neurons belonging to different OEN subnuclei have overlapping targets, indicating that neuromast innervation is not governed by the efferent's soma position (Figures S1D [middle and bottom] and S1E).

Overall, tracing of individual efferent neurons revealed a large degree of divergence that is not somatotopically organized. Since neuromasts in different parts of the body can receive inputs from the same efferent neurons and will experience temporally synchronized stimuli during swimming, it is likely that the efferent mechanisms in place act in bulk rather than being finely tuned to different regions of the body.

In summary, we confirmed the existence of two sources of descending inputs to the neuromasts of zebrafish larvae. The first, the DELL, is a dopaminergic hypothalamic nucleus, and the second, the OEN, is a cholinergic nucleus with further anatomical subdivisions. Both nuclei are anatomically well poised to provide sensory modulation and could transmit efference copy signals to compensate for self-generated stimulation during locomotion.

Functional properties of afferent and efferent neurons during locomotion

Afferent neurons in the PLLg respond to exafferent mechanosensory stimuli, but not to reafferent stimulation

If efference copies act directly on the peripheral sensory pathway rather than at later processing stages, then their effects should be seen in the output of the neurons of the PLLg. To test this hypothesis, we combined stimulus delivery, behavioral tracking, and two-photon imaging of PLLg neurons expressing fluorescent calcium indicators[44] (Figure 2A). Larvae were

Please cite this article in press as: Odstrcil et al., Functional and ultrastructural analysis of reafferent mechanosensation in larval zebrafish, Current Biology (2021), https://doi.org/10.1016/j.cub.2021.11.007

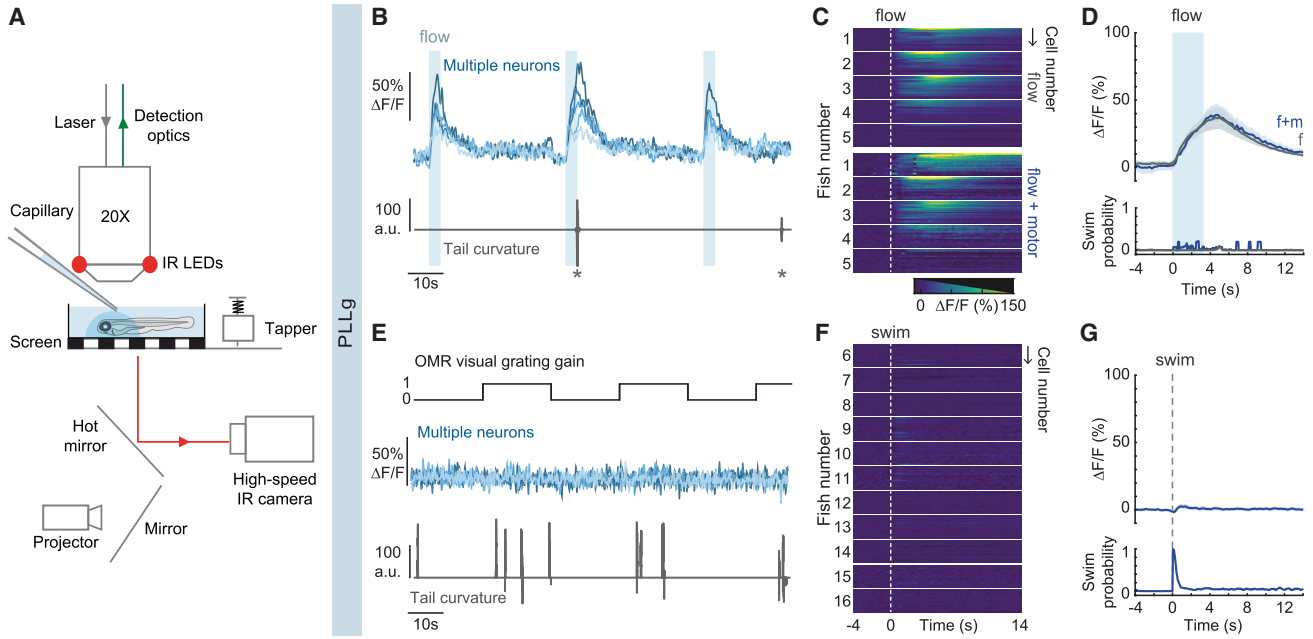

Figure 2. Functional imaging of primary sensory neurons in the PLLg during head-restrained swimming

(A) Experimental setup. Calcium-dependent fluorescence signals are recorded using two2-photon microscopy, and tail position is recorded simultaneously. Visual stimuli are projected under the animal, taps arise from a solenoid, and flow is delivered by pressure injection through a micropipette.

(B) Example traces of top: fluorescence activity (ΔF/F) of flow-responsive neurons in the PLLg of a single GCaMP6s fish (light blue). Bottom: the animal's concomitant cumulative tail curvature. Stars: swim bouts.

(C) Average single-cell responses to 3.3 s of water flow delivery separated into instances that did and did not elicit motor responses. Flow, n = 20, 26, 16, 24, 30 cells in 5 fish; flow + motor, n = 18, 15, 16, 23, 15 cells of the same fish. Dotted line, flow onset. Since stimulus strength was calibrated to trigger behavior stochastically, some neurons were only imaged during flow delivery instances that did not elicit swimming, hence the discrepancy in cell number within individual fish across conditions.

(D) Population average of stimulus-triggered neuronal activity in the PLLg (mean ΔF/F ± SEM) in response to water flow that elicited (f+m, blue) and did not elicit (f, gray) motor responses (n = 5 fish). Averages arise from the single-cell measurements in (C). While the flow delivery period lasted 3.3 s, it is possible that a residual stimulus persisted after delivery was terminated. Bottom: swim probability during the same time period.

(E) Example traces of top: fluorescence activity (ΔF/F) of five neurons in the PLLg of a single fish expressing GCaMP6s. A black and white grating was projected either statically or moving caudo-rostrally with respect to the fish at alternating 20 s intervals to promote swimming. Bottom: concomitant cumulative tail curvature.

(F) Average single-cell responses (ΔF/F) during swim bouts in 11 fish (n = 22, 16, 19, 13, 17, 23, 27, 25, 22, 26, 23 cells). Dotted line, swim starts.

(G) Population swim-triggered averages of neuronal activity in the PLLg (mean ΔF/F ± SEM). Bottom: swim probability during the same period. Averages arise from the single-cell measurements in (F).

See also Figure S2.

restrained in agarose but were free to move their tail. We delivered brief local water injections and observed that, as expected, sensory neurons respond to external flow stimuli (Figures 2B–2D).[45] Previous studies showed that most hair cells of the larval posterior lateral line are tuned to two flow directions, head-to-tail or tail-to-head,[46–48] and that afferent neurons exclusively innervate similarly tuned hair cells.[49–51] Consistent with this anatomical architecture, head-to-tail flow activated only a subset of PLLg sensory neurons, presumably the fraction that is specifically tuned to that direction (Figure 2C). It is worth noting that we used head-to-tail stimulation because this is the main direction of swim-induced flow since larvae rarely swim backward.

In order to dissect the relative contributions of reafferent and exafferent flow stimuli to sensory neuron activity, we adjusted the flow strength to evoke swim events sporadically, enabling us to separate trials into swim and no-swim categories. When swimming occurred during flow delivery, hair cells were stimulated by two separate sources: flow and locomotion. Nonetheless, sensory neuron activity was indistinguishable from that induced by exafferent flow alone (Figures 2C and 2D). This suggests that the reafferent stimulation is balanced by efferent inhibition and that concurrent exafferent flow stimuli can evoke additional activity. In line with this observation, spontaneous swims occurring outside flow delivery periods were not accompanied by a significant rise in PLLg activity (Figures S2A and S2B).

To complement these results, we measured sensory neuron responses during swimming in the absence of exafferent stimulation. Since larvae have a low motor drive in our head-embedded preparation, we used a moving black and white grating to elicit the optomotor response (OMR).[52,53] In this case, the flow patterns detected by the lateral line are exclusively generated by the fish's own motion (reafferent stimulation) (Figure 2E). Remarkably, even though hair cells are strongly deflected by fluid drag during tail undulations, we observed that sensory neurons were not activated by self-induced flow

Please cite this article in press as: Odstrcil et al., Functional and ultrastructural analysis of reafferent mechanosensation in larval zebrafish, Current Biology (2021), https://doi.org/10.1016/j.cub.2021.11.007

(Figures 2F and 2G). Neighboring hindbrain neurons, on the other hand, showed robust motor-locked activity, as expected (Figures S2C and S2D).

These experiments show that while neurons in the PLLg can be activated by exafferent mechanosensory stimuli, they are not excited by hair cell deflections during swims, indicating that efference copy signals exist in the lateral line of larval zebrafish and that these are transmitted directly to the sensory organs.

DELL and OEN neurons exhibit graded motor-correlated activity, while DELL neurons are also activated by sensory stimuli

A hallmark of efference copy signals is their temporal coincidence with motor outputs. We asked if DELL or OEN neurons exhibit this feature by monitoring their activity using the functional imaging assays described above. We used animals expressing pan-neuronal calcium indicators and performed lateral line injections to identify the efferent populations. In addition to OMR-induced swimming, we also studied startle responses. A long-standing hypothesis has proposed that since swims and escapes are governed by distinct motor-command centers,[53–55] they could, in theory, recruit dedicated efferent populations differentially.[56] To address this directly, we evoked startle responses with a mechanical tapper whose strength was again calibrated to evoke responses sporadically.

We found that activity in hypothalamic DELL neurons was locked to the onset of locomotion both during swims and startle responses (Figures 3A, 3B, 3D, S3A, and S3B). Interestingly, DELL neurons were also activated, albeit less strongly, by visual stimuli and taps that did not evoke motor outputs, unmasking a purely sensory component to their activity (Figures 3C, 3D, S3B, and S3C).[57] In line with these results, visually evoked swims elicited a stronger response than spontaneous ones (Figure S3D). To further probe the sensitivity of DELL neurons to other sensory modalities, we delivered flow and heat stimuli. DELL neurons strongly responded to flow, but not to heat, indicating that this nucleus cannot be recruited by all sensory modalities (Figures 3E and 3F). Furthermore, we found that DELL sensitivity to mechanical stimuli also depends on the inner ear, since activation by taps is preserved after specifically ablating the hair cells of the lateral line with copper sulfate (Figure S3E).[58] Finally, hair cell ablation experiments also revealed that even though DELL neurons are flow-sensitive, their activity during locomotion does not result from lateral line reafferent stimulation, since DELL responses during swims are indistinguishable before and after hair cell ablations (Figure S3F).

We next focused our attention on the OEN and observed that these neurons also exhibit elevated activity during swims and startle responses (Figures 3G, 3H, 3J, S3J, and S3K). However, in stark contrast to the DELL, OEN neurons responded exclusively during motor events and were not activated by any sensory stimulus in the absence of locomotion (Figures 3I–3L, S3K, and S3L). Accordingly, lateral line ablations did not affect OEN responses (Figure S3M), and OEN activity was indistinguishable during spontaneous and visually evoked swims (Figure S3N). This pronounced coincidence with—and selectivity for—motor activity provides support for a primary role of this nucleus in efference copy transmission.

Since different behaviors generate different patterns of reafferent stimulation and would thus require different patterns of efferent cancellation, we tested whether the responses of the OEN subnuclei differ when the animal executes distinct motor programs. Apart from the difference in expected reafferent stimulation, these two behaviors are also governed by distinct motor centers. Short-latency (<40 ms) startle responses are generated by Mauthner array cells,[59–61] while routine swims are controlled by other reticulospinal neurons.[53] Therefore, if OEN subnuclei were to respond differentially, this would also imply differences in pre-synaptic inputs. We found that OEN neurons in all subnuclei are synchronously active both during swims and startle responses (Figures S3O and S3P), suggesting that all three subgroups can be considered as one functional unit for the behaviors tested.

Finally, since accurate reafferent cancellation requires matching efferent and reafferent activity patterns, we examined whether increased motor vigor, which naturally elicits stronger reafferent activation, is correlated with stronger corollary neuronal activity in individual efferent neurons. Another possibility is that mechanosensation is completely silenced during locomotion, in which case efferent activity would serve as a gating signal that would not need to be adjusted to the strength of the motor output. We calculated the correlation between swim strength and activity in individual neurons of both efferent nuclei and asked how well various kinematic features match with the strength of efferent activity. Specifically, we correlated total swim power and frequency and amplitude of tail beats with the integral of the fluorescent activity (Figure 3M). All neurons were well correlated with swim power (Figures 3M–3O, S3G, and S3Q), while frequency and amplitude showed much weaker correlation coefficients (Figures S3H, S3I, S3R, and S3S), suggesting that efferent activity scales with total vigor rather than with individual swim components. These results indicate that, already at the zebrafish larval stage, neural mechanisms that allow for a graded subtraction rather than a complete silencing of reafferent sensory signals are in place.

In summary, both DELL and OEN neurons exhibit graded motor-correlated activity during swims and startle responses. DELL neurons, however, are also activated by visual and mechanosensory stimuli, while OEN neurons do not show any sensory-dependent excitation, making them the more likely mediators of efference copies to the lateral line.

Ultrastructure

Our anatomical and functional results show that inputs from the brain reach the lateral line and influence sensory processing. To understand the flow of information within this microcircuit, we set out to determine the precise connectivity patterns of all participating cells and neurites within a neuromast. We collected a complete serial section electron microscopy (ssEM) volume of a neuromast and its surrounding tissue and segmented the entire population of cells and neurites at this convergence zone (Video S1). The animal used expressed red fluorescent protein (RFP) in DELL neurons and GFP in OEN neurons and was imaged using confocal microscopy prior to fixation for EM. These confocal images allowed us to generate a detailed anatomical footprint of each efferent neuron's axonal pattern in the neuromast region. By comparing the fluorescent branching patterns with those of the segmented efferent neurites from the EM volume, we could

Please cite this article in press as: Odstrcil et al., Functional and ultrastructural analysis of reafferent mechanosensation in larval zebrafish, Current Biology (2021), https://doi.org/10.1016/j.cub.2021.11.007

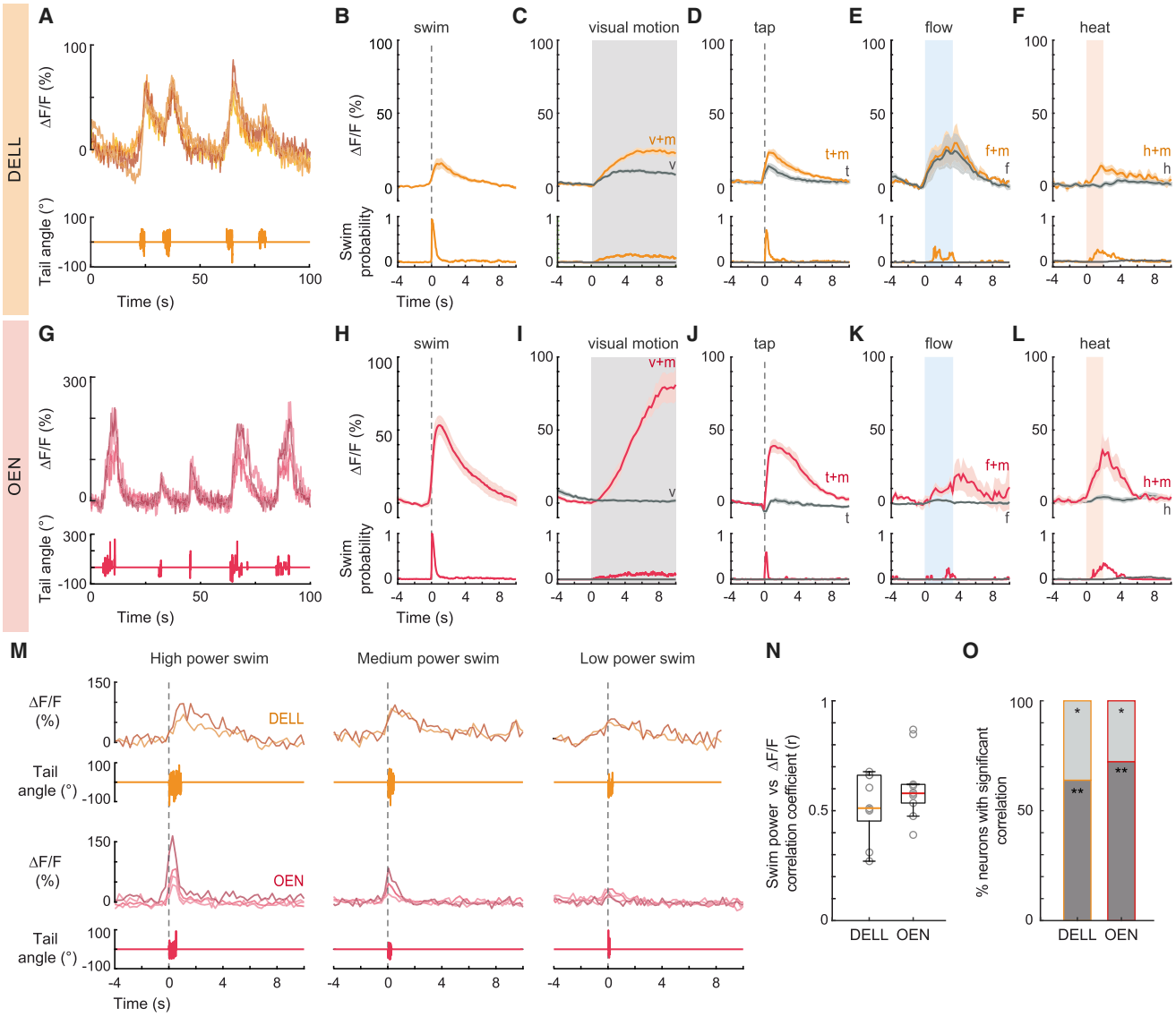

Figure 3. Activity of efferent nuclei during locomotion and in response to diverse sensory stimuli

(A) Example traces of top: fluorescence activity (ΔF/F) of 4 DELL neurons in a single fish. Bottom: the animal's cumulative tail curvature.

(B–F) Top: population activity (mean ΔF/F ± SEM) of neurons in the DELL of GCaMP6s fish. Bottom: swim probability.

(B) Average swim-triggered responses (n = 9 fish).

(C) Average stimulus-triggered responses to moving visual gratings that elicited (v+m, orange) and failed to elicit (v, gray) swimming (n = 11 fish).

(D) Average stimulus-triggered responses to taps that elicited (t+m, orange) and did not elicit (t, gray) swimming (n = 7 fish).

(E) Average stimulus-triggered responses to flow that elicited (f+m, orange) and did not elicit (f, gray) swimming (n = 3 fish).

(F) Average stimulus-triggered responses during heat delivery events that elicited (h+m, orange) and did not elicit (h, gray) swimming (n = 10 fish).

(G) Example traces of top: fluorescence activity (ΔF/F) of 4 OEN neurons in a single fish. Bottom: the animal's tail curvature.

(H–L) Top: population activity (mean ΔF/F ± SEM) of neurons in the OEN of GCaMP6s fish. Bottom: swim probability.

(H) Average swim-triggered responses (n = 8 fish).

(I) Average stimulus-triggered responses to moving visual gratings that elicited (v+m, red) and failed to elicit (v, gray) swimming (n = 7 fish).

(J) Average stimulus-triggered responses to taps that elicited (t+m, red) and did not elicit (t, gray) swimming (n = 5 fish).

(K) Average stimulus-triggered responses to flow that elicited (f+m, red) and did not elicit (f, gray) swimming (n = 5 fish).

(L) Average stimulus-triggered responses during heat delivery events that elicited (h+m, red) and did not elicit (h, gray) swimming (n = 8 fish).

(M) Fluorescence activity (ΔF/F) of single DELL (orange) and OEN (red) neurons during swims of high, medium, and low power (n = 2 DELL and 4 OEN neurons; nuclei imaged in different fish).

(N) Boxplots showing the mean Pearson's coefficients correlating the power of single swim bouts with the concurrent neuronal activity of efferent populations in individual GCaMP6f fish (circles, DELL, n = 9 fish, 2–3 neurons per animal; OEN, n = 10 fish, 2–9 neurons per animal). Medians shown in color. Plots derived from single-neuron analysis shown in Figures S3G and S3Q.

(O) Percentage of cells per fish whose activity was significantly correlated with swim power (DELL, n = 9; OEN, n = 10 fish; **p < 0.001, dark gray; *p < 0.05, light gray).

See also Figure S3.

Please cite this article in press as: Odstrcil et al., Functional and ultrastructural analysis of reafferent mechanosensation in larval zebrafish, Current Biology (2021), https://doi.org/10.1016/j.cub.2021.11.007

unambiguously assign cell-type identities to the segmented structures in the EM dataset (Video S2).

In a single neuromast, we found seven pairs of hair cells of opposing polarity (half rostro-caudal and half caudo-rostral). Since sterocilia in the hair cell bundle increase in length toward the kinocilium, polarity was determined by noting this asymmetry. We also detected multiple neurites: six afferent neurites selectively targeting one of the hair cell polarities, three axonal arbors originating from three separate DELL neurons, and two axonal arbors originating from distinct OEN neurons (Figure 4A; Video S3). Additionally, two neurites lacked counterparts in the confocal microscopy data, so their identities or origin could not be assigned (Video S3). The complete matrix quantifying the pairwise connectivity of all circuit elements is shown in Figure 4G.

Previous ultrastructural studies in zebrafish uncovered that hair cells connect with afferent sensory neurons via ribbon synapses[30,31,62] and that afferent neurons selectively innervate hair cells of a single polarity.[49,50] Our analysis corroborated this specificity: three of the afferent neurites received inputs from rostro-caudally tuned hair cells exclusively, and the other three were targeted by hair cells of the opposite polarity (Figures 4A and 4G).

With respect to efferent innervation, we found that all hair cells receive at least one OEN input. OEN neurons indiscriminately innervate hair cells of both polarities, and partner choices seem to be stochastic: ten of the fourteen hair cells were targeted by one OEN neuron and seven by the other (Figures 4B, 4F, and 4G). On the other hand, and in agreement with previous light-microscopy studies, vesicle-rich DELL terminals are more frequently found in the general vicinity, but not in close apposition to hair cells, often surrounded by support cells (Figures 4C and 4F; Video S3).[63] We only identified a single close-range contact between a DELL axon and a hair cell (Figures 4F and 4G).

Extending our analysis to include afferent neurites as potential targets of efferent innervation, we found that all of the fourteen vesicle-filled profiles from the three DELL axons abut an afferent neurite without discrimination for their target's polarity (Figures 4D and 4G). These profiles exist within the neuromast and also within the axon bundle (Figures 4A, 4C, and 4D). This suggests that the dopaminergic synaptic sites are not necessarily diffuse but can specifically modulate the sensitivity of the initial segment of the sensory dendrites. By contrast, OEN innervation of sensory afferents is less frequent, implying that the role of the OEN is largely dedicated to shaping hair cell sensitivity directly (Figures 4E and 4G). Interestingly, we detected multiple DELL vesicle-filled profiles abutting other DELL and OEN axons, further strengthening the idea of systemic dopaminergic modulation (Figures 4G and S4).

Overall, by combining confocal microscopy with volumetric EM-based segmentation, we enriched ultrastructural datasets that provide nanoscale resolution with fluorescent cellular-identity labels. By determining the small set of connectivity rules in this anatomically complex structure, our approach uncovered a circuit of remarkable functional simplicity: (1) hair cells transmit mechanosensory inputs to afferent neurons in a polarity-specific manner, (2) efferent neurons do not form polarity-specific connections, (3) OEN axons broadly innervate hair cells and some afferent neurites, and (4) DELL vesicle-filled profiles directly abut afferent and some efferent neurites while also terminating at a distance that allows for paracrine modulation of hair cell function.

Circuit perturbations

Afferent neurons of the PLLg acquire motor-evoked responses following ablation of OEN, but not DELL inputs

To test the causal role of DELL and OEN neurons in the modulation of sensory processing during locomotion, we measured the activity of lateral line sensory neurons in the PLLg before and after laser ablation of either efferent population. If any of these nuclei play an essential role in silencing reafferent activity, then their selective removal should relieve the afferent pathway from inhibition and uncover self-evoked activity during locomotion. To quantitatively evaluate the potential consequences of these ablations, we estimated the total number of neurons that comprise each nucleus. By using capture-recapture random sampling, we found that the nuclei are surprisingly small: on average, there are only three to four DELL neurons on each side, while the srOEN, rostral OEN, and caudal OEN contain only one, two, and three neurons on each side, respectively (Figures S5A and S5B). This is an ideal context for targeted ablations since it is easy to remove a significant fraction, if not all, of the neurons in the ensemble (Figure S5C).

To ensure selective ablations, we performed unilateral dye injections in the lateral line nerve and allowed at least 48 h for nerve regeneration.[64,65] This procedure consistently labeled the efferent nuclei, and their distinctive anatomical location allowed for straightforward targeting. Further, since efferent axons do not cross the midline, we imaged PLLg neurons on the contralateral side of the ablation as controls. Removal of DELL neurons did not significantly change PLLg activity during locomotion, indicating that it does not play a role in the selective suppression of reafferent inputs (Figures 5A–5C and S5D). However, response patterns in ipsilateral PLLg neurons displayed a slightly enhanced variability after DELL ablation, as indicated by a qualitative increase in the variance across fish and neurons (Figures 5C and S5D). This suggests that dopamine might have some stabilizing influence, the precise nature of which still needs to be elucidated.

Next, we tested the effect of silencing the OEN efferent pathway on PLLg sensitivity. Before ablations, sensory neurons in the experimental and control ganglia were silent during periods of quiescence and during motor events, as expected (Figures 5D–5F). After OEN ablations, a subset of neurons in the ipsilateral PLLg displayed robust responses during swimming, demonstrating that OEN input is necessary for sensory inhibition during locomotion (Figures 5E, 5F, and S5E [blue]). All neurons of the contralateral ganglion, on the other hand, continued to be silent during swim bouts (Figures 5E, 5F, and S5E [yellow]). The fact that a subset of ipsilateral PLLg neurons remained silent during swims indicates that some inhibition was preserved. This can be explained by the partial and stochastic nature of our method, which, on average, left about three OEN neurons unlabeled and consequently intact in each animal. From the connectivity results in Figure 4, we see that individual hair

Please cite this article in press as: Odstrcil et al., Functional and ultrastructural analysis of reafferent mechanosensation in larval zebrafish, Current Biology (2021), https://doi.org/10.1016/j.cub.2021.11.007

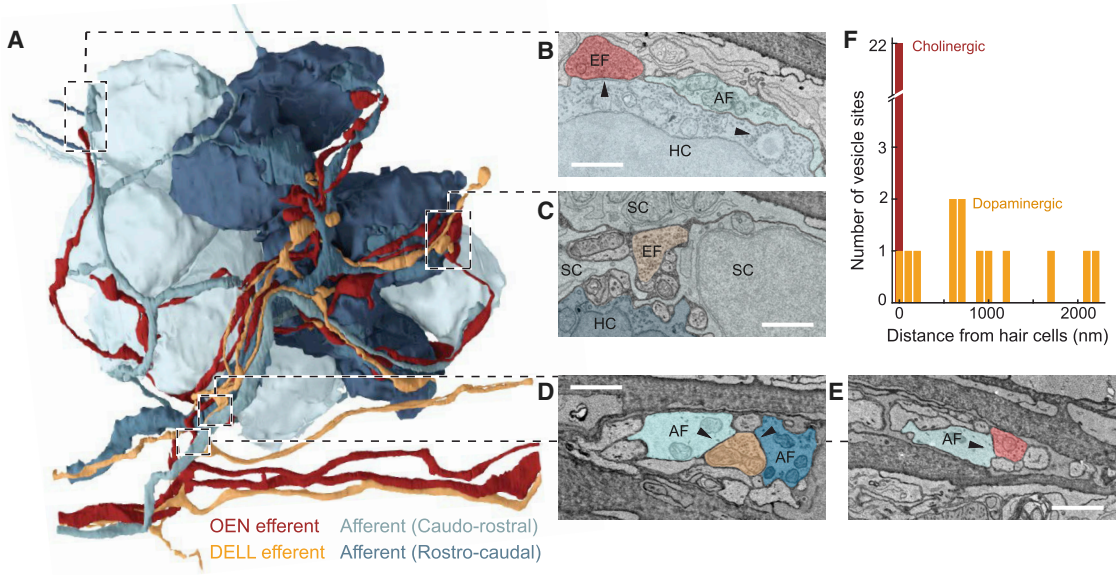

G

Pre-synaptic \ Post-synaptic		Caudo-rostral HC							Rostro-caudal HC							AF			AF			DELL			OEN	
		1	2	3	4	5	6	7	1	2	3	4	5	6	7	1	2	3	4	5	6	1	2	3	1	2
Caudo-rostral HC	1	0	0	0	0	0	0	0	0	0	0	0	0	0	0	0	3	0	0	0	0	0	0	0	0	0
	2	0	0	0	0	0	0	0	0	0	0	0	0	0	0	0	2	0	0	0	0	0	0	0	0	0
	3	0	0	0	0	0	0	0	0	0	0	0	0	0	0	1	2	0	0	0	0	0	0	0	0	0
	4	0	0	0	0	0	0	0	0	0	0	0	0	0	0	1	1	0	0	0	0	0	0	0	0	0
	5	0	0	0	0	0	0	0	0	0	0	0	0	0	0	0	2	0	0	0	0	0	0	0	0	0
	6	0	0	0	0	0	0	0	0	0	0	0	0	0	0	4	0	0	0	0	0	0	0	0	0	0
	7	0	0	0	0	0	0	0	0	0	0	0	0	0	0	2	1	1	0	0	0	0	0	0	0	0
Rostro-caudal HC	1	0	0	0	0	0	0	0	0	0	0	0	0	0	0	0	0	0	3	0	1	0	0	0	0	0
	2	0	0	0	0	0	0	0	0	0	0	0	0	0	0	0	0	0	1	2	0	0	0	0	0	0
	3	0	0	0	0	0	0	0	0	0	0	0	0	0	0	0	0	0	2	0	3	0	0	0	0	0
	4	0	0	0	0	0	0	0	0	0	0	0	0	0	0	0	0	0	1	2	0	0	0	0	0	0
	5	0	0	0	0	0	0	0	0	0	0	0	0	0	0	0	0	0	0	2	0	0	0	0	0	0
	6	0	0	0	0	0	0	0	0	0	0	0	0	0	0	0	0	0	2	2	0	0	0	0	0	0
	7	0	0	0	0	0	0	0	0	0	0	0	0	0	0	0	0	0	1	3	0	0	0	0	0	0
AF	1	0	0	0	0	0	0	0	0	0	0	0	0	0	0	0	0	0	0	0	0	0	0	0	0	0
	2	0	0	0	0	0	0	0	0	0	0	0	0	0	0	0	0	0	0	0	0	0	0	0	0	0
	3	0	0	0	0	0	0	0	0	0	0	0	0	0	0	0	0	0	0	0	0	0	0	0	0	0
AF	4	0	0	0	0	0	0	0	0	0	0	0	0	0	0	0	0	0	0	0	0	0	0	0	0	0
	5	0	0	0	0	0	0	0	0	0	0	0	0	0	0	0	0	0	0	0	0	0	0	0	0	0
	6	0	0	0	0	0	0	0	0	0	0	0	0	0	0	0	0	0	0	0	0	0	0	0	0	0
DELL	1	0	0	0	0	0	0	0	0	0	0	0	0	0	0	4	2	1	0	1	3	0	1	0	2	2
	2	1	0	0	0	0	0	0	0	0	0	0	0	0	0	1	1	0	1	1	1	1	0	0	0	0
	3	0	0	0	0	0	0	0	0	0	0	0	0	0	0	0	2	2	0	2	0	0	0	0	2	0
OEN	1	2	1	1	0	2	1	0	0	2	1	1	3	2	0	0	2	0	1	0	0	0	0	0	0	0
	2	0	0	0	1	1	0	1	1	0	0	1	1	0	2	1	0	2	0	1	1	0	0	0	0	0

Figure 4. Volumetric reconstruction of a PLL neuromast in a 5 dpf fish from ssEM data

(A) Innervation of a PLL neuromast with 14 hair cells belonging to two equal populations of opposing polarities (rostro-caudal and caudo-rostral). Neuron identities were assigned by correlating anatomical ssEM data to fluorescent labeling of efferent types in the same neuromast (Videos S1 and S2).

(B–E) Examples of specific connections (Video S3).

(B) Hair cells (HC) and afferent neurons (AF) connect via ribbon synapses (right arrowhead). An efferent (EF) OEN terminal containing synaptic vesicles contacts the hair cell base containing postsynaptic membrane specializations (left arrowhead).

(C) A vesicle-rich dopaminergic efferent terminal in the proximity of a hair cell. Note the distance between the efferent membrane and the hair cell and the intercalated support cells (SC).

(D) A vesicle-filled profile from a DELL efferent axon within the axon bundle, in close apposition to afferent neurites carrying information from both polarities.

(E) An OEN efferent axon with vesicle release sites, in close apposition to an afferent neurite within the axon bundle that innervates the neuromast.

(F) Histogram showing the distances between DELL (orange) or OEN (red) vesicle sites and the closest hair cell.

(G) Connectivity matrix tallying all synaptic contacts observed in this neuromast.

See also Figure S4.

cells do not receive inputs from all OEN neurons but rather are targeted stochastically by a small subset. Therefore, a partial removal of OEN neurons is expected to uncover activity only in a subset of PLLg neurons and leave the rest fully inhibited. Furthermore, this could also be explained by the observation that, while all neuromast hair cells are mechanosensitive, a fraction are synaptically silent and will fail to excite their postsynaptic afferent partners in response to a stimulus.[66]

Please cite this article in press as: Odstrcil et al., Functional and ultrastructural analysis of reafferent mechanosensation in larval zebrafish, Current Biology (2021), https://doi.org/10.1016/j.cub.2021.11.007

CellPress
OPEN ACCESS

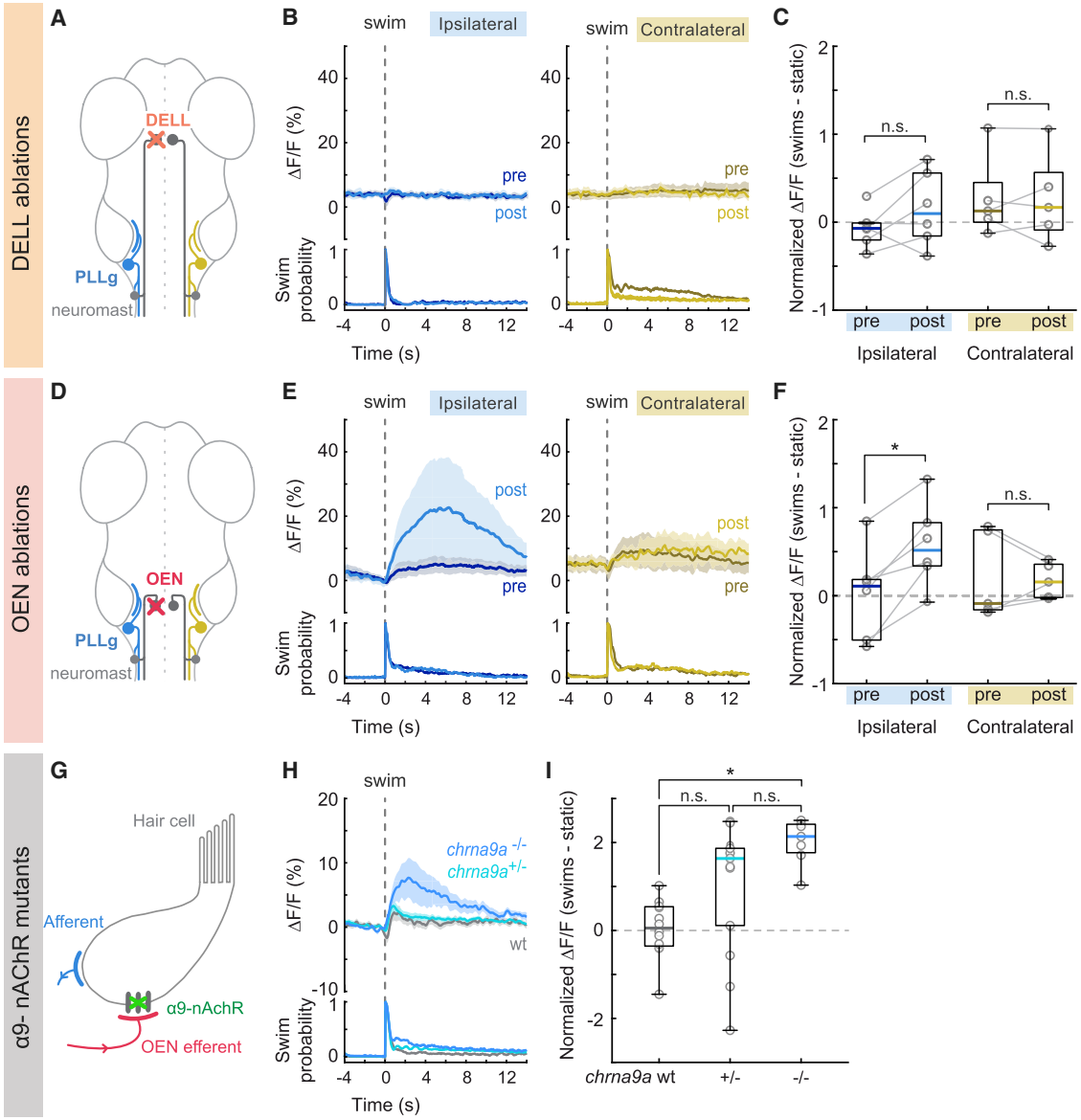

Figure 5. Swim-triggered activity of PLLg neurons after efferent nuclei ablation and in mutants lacking α9-nAChRs

(A) Perturbation schematic. PLLg activity during swims before and after unilateral laser ablation of DELL neurons. Since DELL neurons do not cross the midline, contralateral PLL ganglia serve as controls.

(B) Average swim-triggered responses (mean ΔF/F ± SEM) before and after unilateral DELL ablations in neurons from PLL ganglia in the ipsilateral (left, blue lines) or contralateral (right, yellow lines) side to the ablation. Bottom panels: swim probability (n = 6 and 5 fish).

(C) Boxplots of *Z*-scored population ΔF/F per fish showing the difference in neuronal activity during swimming and quiescent periods of PLL ganglia located ipsilaterally (blue) or contralaterally (yellow) to the ablation site. Medians shown in color. Differences were computed for each fish before and after DELL ablations. Population values correspond to the median of all PLLg neurons for a given fish (individual cell values in Figure S5D). Paired two-tailed Wilcoxon signed-rank test: $p_{ipsilateral} = 0.2188$, $p_{contralateral} = 1$.

(D) Circuit perturbation schematic. PLLg activity during swims before and after unilateral laser ablation of OEN neurons. OEN axons also do not cross the midline, and therefore, contralateral PLL ganglia serve as controls.

(E) Average swim-triggered responses (mean ΔF/F ± SEM) before and after unilateral OEN ablations in neurons from PLL ganglia in the ipsilateral (left, blue lines) or contralateral (right, yellow lines) side to the ablation. Bottom panels: swim probability (n = 6 and 5 fish).

(F) Boxplots of *Z*-scored population ΔF/F per fish showing the difference in neuronal activity during swimming and quiescent periods of PLL ganglia located ipsilaterally (blue) or contralaterally (yellow) to the ablation site. Medians shown in color. Differences were computed for each fish before and after OEN ablations. Population values correspond to the median of all PLLg neurons for a given fish (individual cell values in Figure S5E). Paired two-tailed Wilcoxon signed-rank test: $p_{ipsilateral} = 0.0313$, $p_{contralateral} = 0.8125$.

(G) Perturbation schematic. Hair cells receive cholinergic inputs from OEN efferent neurons (red). If hair cell inhibition is compromised in *chrna9a* mutants, this should be observed in the activity of PLLg neurons.

(legend continued on next page)

Please cite this article in press as: Odstrcil et al., Functional and ultrastructural analysis of reafferent mechanosensation in larval zebrafish, Current Biology (2021), https://doi.org/10.1016/j.cub.2021.11.007

Afferent neurons in the PLLg exhibit motor-evoked stimulation in chrna9a *knockout animals*

In the mammalian cochlea, the inhibitory effect of cholinergic efferents on hair cells is relayed through nicotinic receptor channels composed of $\alpha9/\alpha10$ subunits,[35,36] and efferent suppression of cochlear responses is lost in $\alpha9$ knockout mice.[67] In the hair cells of zebrafish neuromasts, only transcripts of the $\alpha9$ subunit have been detected.[38] We therefore asked whether removal of this receptor subunit would unmask PLLg activity during swim bouts, similar to the effect seen after OEN ablations, and generated *chrna9a* knockout zebrafish using CRISPR-Cas9 genome editing (Figures S5F and S5G). In homozygous *chrna9a* mutants, significant PLLg activity was observed during swim bouts, which was absent in wild-type controls (Figures 5H and 5I). Heterozygous siblings displayed a large variance in PLLg activity across animals, with some animals exhibiting sensory activity during swims and some not. The lack of statistical significance between heterozygotes and their homozygous or wildtype counterparts is likely due to the bi-modal nature of this distribution. We confirmed that the re-emergent activity in the mutant animals originated, as expected, from the hair cells lacking functional nicotinic receptors, since this activity disappeared upon neuromast ablation (Figure S5H). Furthermore, this activity was comparable in size to that observed in OEN-ablated fish (Figures 5E and 5F), suggesting that both these perturbations disrupt the same synaptic pathway.

In summary, there is convergent evidence from ablation and genetic manipulations that the cholinergic efferent pathway plays a critical role in silencing reafferent activity in the lateral line and that this inhibitory action is precisely synchronized with the occurrence of locomotor events. The role of the dopaminergic pathway is less clear. We did not observe any obvious modulatory effects of dopaminergic efferents on sensory neuron activity, but our ultrastructural analysis revealed synaptic contacts between efferent dopaminergic axons and afferent sensory neurites. It is possible that the effects of dopamine occur over longer timespans, which precludes analysis in our experimental settings.

DISCUSSION

Reafferent sensation in any animal is the consequence of a motor action, which is initiated by a neuronal command somewhere in the complex circuitry of the brain. This motor command is readily repurposed to cancel out the expected self-generated stimulation. Understanding the principles behind this mechanism requires investigating it at the structural, functional, and molecular levels. Here, we followed a multi-level approach to dissect the compensatory mechanisms that cancel out reafferent stimulation in the lateral line of zebrafish larvae. This comprehensive line of inquiry has revealed (1) how efferent responses are tuned to motor commands, (2) how synaptic connectivity supports the cancellation of reafferent information, and (3) how specific molecular receptors mediate the required inhibition.

The efferent nuclei

We have observed that the OEN and DELL both fire in strict synchrony with motor actions. However, only the OEN cancels out the predicted reafferent stimulation through direct inhibition of the hair cells via specialized nicotinic receptors.

The exact role of the DELL neurons remains unclear, but their dopaminergic nature along with their targeting of afferent neurites is suggestive of a role in sensory processing modulation. For example, it has been demonstrated that, upon activation by a light flash, dopaminergic neurons in the caudal hypothalamus can enhance the synaptic efficacy between the eighth nerve and the Mauthner cells and consequently increase the probability of subsequent sound-induced startle responses.[68] Specifically in the lateral line, previous work has shown that dopamine can have a sensitizing effect on neuromast hair cells via the D1b receptor.[63] The authors, however, did not detect D1b receptor expression in any of the neurons that innervate hair cells, so the molecular players in the synapses between DELL axons and afferent neurites are still unknown. Since DELL neurons exhibit increased activity during locomotion, and in response to sensory stimuli such as moving visual gratings, flow, and taps (Figures 3A–3F), their effects depended on both motor state and sensory stimulation.[57] The source of this motor-locked activity is unknown. We cannot distinguish whether this is a true copy of the motor command or whether it is a reafferent signal from sensory modalities other than the lateral line that can be activated during locomotion, such as proprioception, somatosensation, or the inner ear.

By acting through G protein-coupled receptors, the effects of dopamine likely outlast the brief occurrences of swims or stimuli—leaving the sensory system in a more receptive state during the inter-bout periods or following stimuli that might require subsequent behavioral responses. Additionally, DELL neurons send collaterals to the spinal cord and have been shown to affect bout frequency, indicating a role in the regulation of spinal circuit excitability.[42,69] Taken together, these observations suggest that DELL neurons serve a dual function in the control of basal threshold levels of both sensory and motor networks.

OEN neurons, on the other hand, transmit inhibitory efference copy signals directly onto hair cells to cancel out reafferent stimuli during locomotion.[27,28] Without such inhibition, hair cells habituate readily, which can render the animal insensitive to exafferent cues.[70] Interestingly, individual OEN neurons broadcast their inhibitory signals to the lateral line and the inner ear, such that this small population is used ubiquitously to cancel reafferent information in all sensory modalities that depend on hair cell function (Figures S1D and S1E). This simple strategy prevents informational ambiguity and most likely serves to suppress maladaptive triggering of behavioral responses.

(H) Average swim-triggered responses (mean ΔF/F ± SEM) of PLLg neurons in *chrna9aΔ1049* homozygous (blue) and heterozygous (cyan) siblings and wild-type controls (wt, gray) (n = 8, 14, 12 fish). Wild-type fish correspond to one wild-type sibling and all animals from Figure 2F. Bottom: swim probability.

(I) Boxplots of *Z*-scored population ΔF/F per fish showing the difference in neuronal activity during swimming and quiescent periods in wild-type and mutant animals. Medians shown in color. Kruskal-Wallis one-way analysis of variance, p = 0.0010. Unpaired two-tailed Wilcoxon rank-sum test with post hoc Bonferroni correction, $p_{wt:+/-} = 0.0252$; $p_{+/-:-/-} = 0.0676$; $p_{wt:-/-} = 3.9692 \times 10^{-5}$.

See also Figure S5.

Please cite this article in press as: Odstrcil et al., Functional and ultrastructural analysis of reafferent mechanosensation in larval zebrafish, Current Biology (2021), https://doi.org/10.1016/j.cub.2021.11.007

Subtraction versus silencing

Mechanistically, reafferent cancellation could be achieved by a precise subtraction of the predicted reafferent signals during locomotion or by a complete shunting of hair cell excitability. The former requires a finely tuned inhibition that matches the strength of the reafferent signal, which in turn depends on the strength of the motor command. An exact subtraction of the reafferent signal, whose precision would need to be homeostatically adjusted to account for changes in the body of the animal[71] or the properties of the environment,[10,14,72] would allow for the detection of concomitant external cues, a necessity when animals move continuously and not in intermittent bouts. Since zebrafish transition from bout swimming to continuous locomotion during later stages in development, mechanisms might already be in place in the larvae that favor subtraction over complete suppression. Our findings argue that the fundamental properties for subtraction are already in place. First, we observe that sensory neurons in the PLLg respond to exafferent flow stimulation during a swim and that, therefore, the animal is not "blind" during locomotion (Figure 2D). Second, we show that OEN activity is highly correlated with the strength of motor output, consistent with a graded inhibition of the corresponding reafferent stimulation (Figures 3N, 3O, and S3Q). Additionally, it has been shown that efferent inhibition of the neuromast in larval zebrafish is stronger in hair cells that are activated by forward motion and that hair cells tuned to other perturbations are less affected.[27] Together, this suggests a selective tailoring of the inhibition to suppress motion-specific activation, a feature that will become necessary when the animal starts swimming continuously and the reafferent stimulus becomes complex and long-lasting.

The connectome of the neuromast

Seminal work provided the first EM images of a larval zebrafish neuromast and established the existence of synaptic connections between hair cells and sensory afferents and between efferents and hair cells.[30,31] Subsequently, a comprehensive ultrastructural analysis of zebrafish neuromasts performed at an early developmental stage (~3 dpf) rendered a first sketch of this interconnected microcircuit.[62] In line with these studies, we confirm the close apposition of afferent terminals to ribbon synapses, as well as the precise selectivity of individual afferent neurons to hair cells of one specific polarity. However, Dow et al.[62] found that in most neuromasts, a single efferent neurite contacts all hair cells of both polarities. In contrast, we find that multiple neurites of different types target some, but not all, hair cells or afferent neurites (Figure 4G). This discrepancy can be reconciled by differences in age: at 3 dpf, connectivity patterns might be less refined, as is commonly observed in other developing neural structures such as the neuromuscular junction.[73]

Since cholinergic terminals form direct synapses onto hair cells, the average distance between their respective membranes was, as expected, less than 100 nm (Figure 4F). For the majority of dopaminergic release sites, this distance exceeded 500 nm. This suggested, at first glance and in line with previous work,[63] that dopamine is released from diffuse synapses into the extracellular space of this densely interconnected region. However, upon closer examination of the complete reconstruction, we find that individual dopaminergic neurites appear to specifically target afferent terminals, regardless of the polarity of their targets. Moreover, we have also uncovered axo-axonic connections between DELL neurons and other DELL or OEN axons (Figures 4G and S4). The nature and function of these dopaminergic connections remain to be elucidated.

α9-nAChR gene knockouts

Our experiments using knockout larvae establish that the α9 cholinergic receptor subunit, which is also conserved in the hair cells of the mammalian inner ear, is pivotal for the suppression of reafferent mechanosensation in the neuromast. Recent work has determined that α9 subunits are expressed in zebrafish neuromasts and that these can form functional homomeric acetylcholine-sensitive receptors in heterologous preparations.[32] Furthermore, using calcium imaging, this study showed that application of acetylcholine reduces calcium signals evoked by hair cell stimulation and that this effect is blocked by apamin, a selective blocker of small-conductance calcium-activated potassium (SK) channels. The emerging view is that reafferent inhibition relies on acetylcholine-mediated calcium entry through α9 receptors, which subsequently activates calcium-dependent SK channels to hyperpolarize the hair cells. Whether this mechanism is also true for the inhibition of afferent neurites remains to be determined. These observations are also consistent with results from the lateral line of *Xenopus laevis*[33] and underscore the usefulness of the lateral line of aquatic organisms as a more accessible model system for further studies of vertebrate hair cell function in the context of human inner ear pathologies.

A complete model of local microcircuitry

We show that larval zebrafish possess parallel descending inputs that can differentially influence mechanosensory processing in the peripheral sensory pathway. Cholinergic signals from the hindbrain transmit efference copy signals that cancel out self-generated stimulation during locomotion, while dopaminergic signals from the hypothalamus may have a more complex role in modulating sensitivity in a broader behavioral context. These results allow us to propose a complete model—spanning circuit connectivity, neuronal function, and synaptic receptors—of the circuit underlying reafferent mechanosensation in larval zebrafish.

STAR★METHODS

Detailed methods are provided in the online version of this paper and include the following:

- KEY RESOURCES TABLE
- RESOURCE AVAILABILITY
  - Lead contact
  - Materials availability
  - Data and code availability
- EXPERIMENTAL MODEL AND SUBJECT DETAILS
  - Zebrafish
- METHOD DETAILS
  - Dye labeling of efferent neurons
  - Capture-recapture random sampling
  - Immunohistochemistry
  - Confocal imaging
  - Focal electroporations

- *In vivo* 2-photon functional imaging
- Behavioral tracking during functional imaging
- Stimulus delivery during functional imaging
- Chemical ablation of neuromasts
- Tissue preparation for ssSEM
- Volumetric reconstructions from ssEM data
- Laser ablations of efferent nuclei
- Generation of chrna9a mutants using CRISPR–Cas9

● QUANTIFICATION AND STATISTICAL ANALYSIS

- Data analysis
- Statistical analysis

SUPPLEMENTAL INFORMATION

Supplemental information can be found online at https://doi.org/10.1016/j.cub.2021.11.007.

ACKNOWLEDGMENTS

We thank Jessica Miller and Karen Hurley for fish care, Douglas Richardson and the Harvard Center for Biological Imaging for microscopy advice, and Renate Hellmiss and Mariana Grünthal for graphic design support. We are grateful to Isaac Bianco, Alex Schier, Nao Uchida, Aravi Samuel, and Chris Harvey for valuable discussions; Polina Kehayova for resource management; and Eva Naumann, Julian Arni, and Baba Yogesh for critical reading of the manuscript. This research was supported by the National Institutes of Health (U19NS104653, R43 OD024879, and 2R44OD024879), the National Science Foundation (IIS-1912293), the Simons Foundation (SCGB 542973), and the Human Frontier Science Program (RGP0033/2014) awarded to F.E. I.O. was supported by the Human Frontier Science Program (LT000805/2019-L) and the European Molecular Biology Organization (ALTF 202-2019). R.P. was supported by the Max Planck Foundation and by the Deutsche Forschungsgemeinschaft (DFG, German Research Foundation) under Germany's Excellence Strategy within the framework of the Munich Cluster for Systems Neurology (EXC 2145 SyN-ergy – ID 390857198).

AUTHOR CONTRIBUTIONS

I.O. and F.E. designed the experiments with contributions from R.P., M.H., and P.O. I.O. performed the experiments, using software written by R.P. in the behavioral setup and with M.H. for experiments with heat delivery and M.N. with flow. M.D.P. obtained and analyzed the neuromast connectome with support from J.B.-W. for tissue preparation and tracing, J.B.-W. and R.S. for data acquisition, A.P. for image alignment and volume reconstruction, and J.W.L. for infrastructure and supervision. J.A.G. generated the *chrna9a* mutants. I.O. analyzed the data and wrote the paper with F.E. All authors read and commented on the manuscript.

DECLARATION OF INTERESTS

The authors declare no competing interests.

Received: May 4, 2021
Revised: August 17, 2021
Accepted: November 3, 2021
Published: November 24, 2021

REFERENCES

1. von Helmholtz, H. (1867). Handbuch der physiologischen Optik (Voss).
2. Crapse, T.B., and Sommer, M.A. (2008). Corollary discharge across the animal kingdom. Nat. Rev. Neurosci. *9*, 587–600.
3. Cullen, K.E. (2004). Sensory signals during active versus passive movement. Curr. Opin. Neurobiol. *14*, 698–706.
4. Straka, H., Simmers, J., and Chagnaud, B.P. (2018). A new perspective on predictive motor signaling. Curr. Biol. *28*, R232–R243.
5. Keller, G.B., and Hahnloser, R.H. (2009). Neural processing of auditory feedback during vocal practice in a songbird. Nature *457*, 187–190.
6. Schneider, D.M., Nelson, A., and Mooney, R. (2014). A synaptic and circuit basis for corollary discharge in the auditory cortex. Nature *513*, 189–194.
7. Schneider, D.M., Sundararajan, J., and Mooney, R. (2018). A cortical filter that learns to suppress the acoustic consequences of movement. Nature *561*, 391–395.
8. Perks, K.E., Krotinger, A., and Bodznick, D. (2020). A cerebellum-like circuit in the lateral line system of fish cancels mechanosensory input associated with its own movements. J. Exp. Biol. *223*, jeb204438.
9. Bryan, J.S., and Krasne, F.B. (1977). Presynaptic inhibition: the mechanism of protection from habituation of the crayfish lateral giant fibre escape response. J. Physiol. *271*, 369–390.
10. Kim, A.J., Fitzgerald, J.K., and Maimon, G. (2015). Cellular evidence for efference copy in Drosophila visuomotor processing. Nat. Neurosci. *18*, 1247–1255.
11. Sperry, R.W. (1950). Neural basis of the spontaneous optokinetic response produced by visual inversion. J. Comp. Physiol. Psychol. *43*, 482–489.
12. von Holst, E., and Mittelstaedt, H. (1950). Das Reafferenzprinzip. Naturwissenschaften *37*, 464–476.
13. Zipser, B., and Bennett, M.V. (1976). Interaction of electrosensory and electromotor signals in lateral line lobe of a mormyrid fish. J. Neurophysiol. *39*, 713–721.
14. Bell, C.C. (1981). An efference copy which is modified by reafferent input. Science *214*, 450–453.
15. Montgomery, J.C., and Bodznick, D. (1994). An adaptive filter that cancels self-induced noise in the electrosensory and lateral line mechanosensory systems of fish. Neurosci. Lett. *174*, 145–148.
16. Dijkgraaf, S. (1963). The functioning and significance of the lateral-line organs. Biol. Rev. Camb. Philos. Soc. *38*, 51–105.
17. Pitcher, T.J., Partridge, B.L., and Wardle, C.S. (1976). A blind fish can school. Science *194*, 963–965.
18. Montgomery, J.C., Macdonald, F., Baker, C.F., and Carton, A.G. (2002). Hydrodynamic contributions to multimodal guidance of prey capture behavior in fish. Brain Behav. Evol. *59*, 190–198.
19. Stewart, W.J., and McHenry, M.J. (2010). Sensing the strike of a predator fish depends on the specific gravity of a prey fish. J. Exp. Biol. *213*, 3769–3777.
20. Suli, A., Watson, G.M., Rubel, E.W., and Raible, D.W. (2012). Rheotaxis in larval zebrafish is mediated by lateral line mechanosensory hair cells. PLoS ONE *7*, e29727.
21. Oteiza, P., Odstrcil, I., Lauder, G., Portugues, R., and Engert, F. (2017). A novel mechanism for mechanosensory-based rheotaxis in larval zebrafish. Nature *547*, 445–448.
22. Cahn, P.H., and Shaw, E. (1965). A method for studying lateral line cupular bending in juvenile fishes. Bull. Mar. Sci. *15*, 1060–1071.
23. Russell, I.J. (1971). The role of the lateral-line efferent system in Xenopus laevis. J. Exp. Biol. *54*, 621–641.
24. Chagnaud, B.P., Banchi, R., Simmers, J., and Straka, H. (2015). Spinal corollary discharge modulates motion sensing during vertebrate locomotion. Nat. Commun. *6*, 7982.
25. Russell, I.J., and Roberts, B.L. (1974). Active reduction of lateral-line sensitivity in swimming dogfish. J. Comp. Physiol. *94*, 7–15.
26. Russell, I.J. (1976). Central inhibition of lateral line input in the medulla of the goldfish by neurones which control active body movements. J. Comp. Physiol. *111*, 335–358.
27. Pichler, P., and Lagnado, L. (2020). Motor behavior selectively inhibits hair cells activated by forward motion in the lateral line of zebrafish. Curr. Biol. *30*, 150–157.e3.

28. Lunsford, E.T., Skandalis, D.A., and Liao, J.C. (2019). Efferent modulation of spontaneous lateral line activity during and after zebrafish motor commands. J. Neurophysiol. *122*, 2438–2448.

29. Coombs, S., Görner, P., and Münz, H. (2012). The Mechanosensory Lateral Line: Neurobiology and Evolution (Springer Science & Business Media).

30. Metcalfe, W.K., Kimmel, C.B., and Schabtach, E. (1985). Anatomy of the posterior lateral line system in young larvae of the zebrafish. J. Comp. Neurol. *233*, 377–389.

31. Bricaud, O., Chaar, V., Dambly-Chaudière, C., and Ghysen, A. (2001). Early efferent innervation of the zebrafish lateral line. J. Comp. Neurol. *434*, 253–261.

32. Carpaneto Freixas, A.E., Moglie, M.J., Castagnola, T., Salatino, L., Domene, S., Marcovich, I., Gallino, S., Wedemeyer, C., Goutman, J.D., Plazas, P.V., and Elgoyhen, A.B. (2021). Unraveling the molecular players at the cholinergic efferent synapse of the zebrafish lateral line. J. Neurosci. *41*, 47–60.

33. Dawkins, R., Keller, S.L., and Sewell, W.F. (2005). Pharmacology of acetylcholine-mediated cell signaling in the lateral line organ following efferent stimulation. J. Neurophysiol. *93*, 2541–2551.

34. Poppi, L.A., Holt, J.C., Lim, R., and Brichta, A.M. (2020). A review of efferent cholinergic synaptic transmission in the vestibular periphery and its functional implications. J. Neurophysiol. *123*, 608–629.

35. Elgoyhen, A.B., Johnson, D.S., Boulter, J., Vetter, D.E., and Heinemann, S. (1994). Alpha 9: an acetylcholine receptor with novel pharmacological properties expressed in rat cochlear hair cells. Cell *79*, 705–715.

36. Elgoyhen, A.B., Vetter, D.E., and Katz, E. (2001). a10: a determinant of nicotinic cholinergic receptor function in mammalian vestibular and cochlear mechanosensory hair cells. Proc. Natl. Acad. Sci. USA *98*, 3501–3506. PubMed.

37. Taranda, J., Maison, S.F., Ballestero, J.A., Katz, E., Savino, J., Vetter, D.E., Boulter, J., Liberman, M.C., Fuchs, P.A., and Elgoyhen, A.B. (2009). A point mutation in the hair cell nicotinic cholinergic receptor prolongs cochlear inhibition and enhances noise protection. PLoS Biol. *7*, e18.

38. Erickson, T., and Nicolson, T. (2015). Identification of sensory hair-cell transcripts by thiouracil-tagging in zebrafish. BMC Genomics *16*, 842.

39. Xi, Y., Yu, M., Godoy, R., Hatch, G., Poitras, L., and Ekker, M. (2011). Transgenic zebrafish expressing green fluorescent protein in dopaminergic neurons of the ventral diencephalon. Dev. Dyn. *240*, 2539–2547.

40. Haehnel-Taguchi, M., Fernandes, A.M., Böhler, M., Schmitt, I., Tittel, L., and Driever, W. (2018). Projections of the diencephalospinal dopaminergic system to peripheral sense organs in larval zebrafish (*Danio rerio*). Front. Neuroanat. *12*, 20.

41. Tay, T.L., Ronneberger, O., Ryu, S., Nitschke, R., and Driever, W. (2011). Comprehensive catecholaminergic projectome analysis reveals single-neuron integration of zebrafish ascending and descending dopaminergic systems. Nat. Commun. *2*, 171.

42. Jay, M., De Faveri, F., and McDearmid, J.R. (2015). Firing dynamics and modulatory actions of supraspinal dopaminergic neurons during zebrafish locomotor behavior. Curr. Biol. *25*, 435–444.

43. McPherson, A.D., Barrios, J.P., Luks-Morgan, S.J., Manfredi, J.P., Bonkowsky, J.L., Douglass, A.D., and Dorsky, R.I. (2016). Motor behavior mediated by continuously generated dopaminergic neurons in the zebrafish hypothalamus recovers after cell ablation. Curr. Biol. *26*, 263–269.

44. Chen, T.-W., Wardill, T.J., Sun, Y., Pulver, S.R., Renninger, S.L., Baohan, A., Schreiter, E.R., Kerr, R.A., Orger, M.B., Jayaraman, V., et al. (2013). Ultrasensitive fluorescent proteins for imaging neuronal activity. Nature *499*, 295–300.

45. Liao, J.C. (2010). Organization and physiology of posterior lateral line afferent neurons in larval zebrafish. Biol. Lett. *6*, 402–405.

46. López-Schier, H., Starr, C.J., Kappler, J.A., Kollmar, R., and Hudspeth, A.J. (2004). Directional cell migration establishes the axes of planar polarity in the posterior lateral-line organ of the zebrafish. Dev. Cell *7*, 401–412.

47. Ghysen, A., and Dambly-Chaudière, C. (2007). The lateral line microcosmos. Genes Dev. *21*, 2118–2130.

48. Pichler, P., and Lagnado, L. (2019). The transfer characteristics of hair cells encoding mechanical stimuli in the lateral line of zebrafish. J. Neurosci. *39*, 112–124.

49. Nagiel, A., Andor-Ardó, D., and Hudspeth, A.J. (2008). Specificity of afferent synapses onto plane-polarized hair cells in the posterior lateral line of the zebrafish. J. Neurosci. *28*, 8442–8453.

50. Faucherre, A., Pujol-Martí, J., Kawakami, K., and López-Schier, H. (2009). Afferent neurons of the zebrafish lateral line are strict selectors of hair-cell orientation. PLoS ONE *4*, e4477.

51. Dow, E., Siletti, K., and Hudspeth, A.J. (2015). Cellular projections from sensory hair cells form polarity-specific scaffolds during synaptogenesis. Genes Dev. *29*, 1087–1094.

52. Neuhauss, S.C., Biehlmaier, O., Seeliger, M.W., Das, T., Kohler, K., Harris, W.A., and Baier, H. (1999). Genetic disorders of vision revealed by a behavioral screen of 400 essential loci in zebrafish. J. Neurosci. *19*, 8603–8615.

53. Orger, M.B., Kampff, A.R., Severi, K.E., Bollmann, J.H., and Engert, F. (2008). Control of visually guided behavior by distinct populations of spinal projection neurons. Nat. Neurosci. *11*, 327–333.

54. Severi, K.E., Portugues, R., Marques, J.C., O'Malley, D.M., Orger, M.B., and Engert, F. (2014). Neural control and modulation of swimming speed in the larval zebrafish. Neuron *83*, 692–707.

55. Ritter, D.A., Bhatt, D.H., and Fetcho, J.R. (2001). In vivo imaging of zebrafish reveals differences in the spinal networks for escape and swimming movements. J. Neurosci. *21*, 8956–8965.

56. Kimmel, C.B., Patterson, J., and Kimmel, R.O. (1974). The development and behavioral characteristics of the startle response in the zebra fish. Dev. Psychobiol. *7*, 47–60.

57. Reinig, S., Driever, W., and Arrenberg, A.B. (2017). The descending diencephalic dopamine system is tuned to sensory stimuli. Curr. Biol. *27*, 318–333.

58. Lacoste, A.M.B., Schoppik, D., Robson, D.N., Haesemeyer, M., Portugues, R., Li, J.M., Randlett, O., Wee, C.L., Engert, F., and Schier, A.F. (2015). A convergent and essential interneuron pathway for Mauthner-cell-mediated escapes. Curr. Biol. *25*, 1526–1534.

59. O'Malley, D.M., Kao, Y.H., and Fetcho, J.R. (1996). Imaging the functional organization of zebrafish hindbrain segments during escape behaviors. Neuron *17*, 1145–1155.

60. Foreman, M.B., and Eaton, R.C. (1993). The direction change concept for reticulospinal control of goldfish escape. J. Neurosci. *13*, 4101–4113.

61. Liu, K.S., and Fetcho, J.R. (1999). Laser ablations reveal functional relationships of segmental hindbrain neurons in zebrafish. Neuron *23*, 325–335.

62. Dow, E., Jacobo, A., Hossain, S., Siletti, K., and Hudspeth, A.J. (2018). Connectomics of the zebrafish's lateral-line neuromast reveals wiring and miswiring in a simple microcircuit. eLife *7*, e33988.

63. Toro, C., Trapani, J.G., Pacentine, I., Maeda, R., Sheets, L., Mo, W., and Nicolson, T. (2015). Dopamine modulates the activity of sensory hair cells. J. Neurosci. *35*, 16494–16503.

64. Villegas, R., Martin, S.M., O'Donnell, K.C., Carrillo, S.A., Sagasti, A., and Allende, M.L. (2012). Dynamics of degeneration and regeneration in developing zebrafish peripheral axons reveals a requirement for extrinsic cell types. Neural Dev. *7*, 19.

65. Pujol-Martí, J., Faucherre, A., Aziz-Bose, R., Asgharsharghi, A., Colombelli, J., Trapani, J.G., and López-Schier, H. (2014). Converging axons collectively initiate and maintain synaptic selectivity in a constantly remodeling sensory organ. Curr. Biol. *24*, 2968–2974.

66. Zhang, Q., Li, S., Wong, H.C., He, X.J., Beirl, A., Petralia, R.S., Wang, Y.-X., and Kindt, K.S. (2018). Synaptically silent sensory hair cells in zebrafish are recruited after damage. Nat. Commun. *9*, 1388.

67. Vetter, D.E., Liberman, M.C., Mann, J., Barhanin, J., Boulter, J., Brown, M.C., Saffiote-Kolman, J., Heinemann, S.F., and Elgoyhen, A.B. (1999).

Role of alpha9 nicotinic ACh receptor subunits in the development and function of cochlear efferent innervation. Neuron *23*, 93–103.

68. Mu, Y., Li, X.-Q., Zhang, B., and Du, J.-L. (2012). Visual input modulates audiomotor function via hypothalamic dopaminergic neurons through a cooperative mechanism. Neuron *75*, 688–699.
69. Barrios, J.P., Wang, W.-C., England, R., Reifenberg, E., and Douglass, A.D. (2020). Hypothalamic dopamine neurons control sensorimotor behavior by modulating brainstem premotor nuclei in zebrafish. Curr. Biol. *30*, 4606–4618.e4.
70. Skandalis, D.A., Lunsford, E.T., and Liao, J. (2021). Corollary discharge prevents signal distortion and enhances sensing during locomotion. bioRxiv. https://doi.org/10.1101/2021.02.15.431323.
71. von Uckermann, G., Lambert, F.M., Combes, D., Straka, H., and Simmers, J. (2016). Adaptive plasticity of spino-extraocular motor coupling during locomotion in metamorphosing Xenopus laevis. J. Exp. Biol. *219*, 1110–1121.
72. Bodznick, D., Montgomery, J.C., and Carey, M. (1999). Adaptive mechanisms in the elasmobranch hindbrain. J. Exp. Biol. *202*, 1357–1364.
73. Tapia, J.C., Wylie, J.D., Kasthuri, N., Hayworth, K.J., Schalek, R., Berger, D.R., Guatimosim, C., Seung, H.S., and Lichtman, J.W. (2012). Pervasive synaptic branch removal in the mammalian neuromuscular system at birth. Neuron *74*, 816–829.
74. Kim, D.H., Kim, J., Marques, J.C., Grama, A., Hildebrand, D.G.C., Gu, W., Li, J.M., and Robson, D.N. (2017). Pan-neuronal calcium imaging with cellular resolution in freely swimming zebrafish. Nat. Methods *14*, 1107–1114.
75. Higashijima, S., Hotta, Y., and Okamoto, H. (2000). Visualization of cranial motor neurons in live transgenic zebrafish expressing green fluorescent protein under the control of the islet-1 promoter/enhancer. J. Neurosci. *20*, 206–218.
76. Wen, L., Wei, W., Gu, W., Huang, P., Ren, X., Zhang, Z., Zhu, Z., Lin, S., and Zhang, B. (2008). Visualization of monoaminergic neurons and neurotoxicity of MPTP in live transgenic zebrafish. Dev. Biol. *314*, 84–92.
77. Xiao, T., Roeser, T., Staub, W., and Baier, H. (2005). A GFP-based genetic screen reveals mutations that disrupt the architecture of the zebrafish retinotectal projection. Development *132*, 2955–2967.
78. Randlett, O., Wee, C.L., Naumann, E.A., Nnaemeka, O., Schoppik, D., Fitzgerald, J.E., Portugues, R., Lacoste, A.M.B., Riegler, C., Engert, F., and Schier, A.F. (2015). Whole-brain activity mapping onto a zebrafish brain atlas. Nat. Methods *12*, 1039–1046.
79. Wee, Song, C.L., Nikitchenko, E.,M., Herrera, K.J., Wong, S., Engert, F., and Kunes, S. (2021). Social isolation modulates appetite and defensive behavior via a common oxytocinergic circuit in larval zebrafish. bioRxiv. https://doi.org/10.1101/2020.02.19.956854.
80. Labun, K., Montague, T.G., Gagnon, J.A., Thyme, S.B., and Valen, E. (2016). CHOPCHOP v2: a web tool for the next generation of CRISPR genome engineering. Nucleic Acids Res. *44* (W1), W272-6.
81. Lister, J.A., Robertson, C.P., Lepage, T., Johnson, S.L., and Raible, D.W. (1999). nacre encodes a zebrafish microphthalmia-related protein that regulates neural-crest-derived pigment cell fate. Development *126*, 3757–3767.
82. Chapman, D.G. (1954). The estimation of biological populations. The Annals of Mathematical Statistics *25*, 1–15.
83. Inoue, D., and Wittbrodt, J. (2011). One for all–a highly efficient and versatile method for fluorescent immunostaining in fish embryos. PLoS ONE *6*, e19713.
84. Tawk, M., Bianco, I.H., and Clarke, J.D.W. (2009). Focal electroporation in zebrafish embryos and larvae. Methods Mol. Biol. *546*, 145–151.
85. Portugues, R., and Engert, F. (2011). Adaptive locomotor behavior in larval zebrafish. Front. Syst. Neurosci. *5*, 72.
86. Haesemeyer, M., Robson, D.N., Li, J.M., Schier, A.F., and Engert, F. (2018). A brain-wide circuit model of heat-evoked swimming behavior in larval zebrafish. Neuron *98*, 817–831.e6.
87. Schuster, K., and Ghysen, A. (2013). Labeling hair cells and afferent neurons in the posterior lateral-line system of zebrafish. Cold Spring Harb. Protoc. *2013*, 1172–1174.
88. Ma, L.-H., Gilland, E., Bass, A.H., and Baker, R. (2010). Ancestry of motor innervation to pectoral fin and forelimb. Nat. Commun. *1*, 49.
89. Hildebrand, D.G.C., Cicconet, M., Torres, R.M., Choi, W., Quan, T.M., Moon, J., Wetzel, A.W., Scott Champion, A., Graham, B.J., Randlett, O., et al. (2017). Whole-brain serial-section electron microscopy in larval zebrafish. Nature *545*, 345–349.
90. Saalfeld, S., Fetter, R., Cardona, A., and Tomancak, P. (2012). Elastic volume reconstruction from series of ultra-thin microscopy sections. Nat. Methods *9*, 717–720.
91. Gagnon, J.A., Valen, E., Thyme, S.B., Huang, P., Akhmetova, L., Pauli, A., Montague, T.G., Zimmerman, S., Richter, C., and Schier, A.F. (2014). Efficient mutagenesis by Cas9 protein-mediated oligonucleotide insertion and large-scale assessment of single-guide RNAs. PLoS ONE *9*, e98186.
92. Berger, D.R., Seung, H.S., and Lichtman, J.W. (2018). VAST (volume annotation and segmentation tool): efficient manual and semi-automatic labeling of large 3D image stacks. Front. Neural Circuits *12*, 88.
93. Ahrens, M.B., Li, J.M., Orger, M.B., Robson, D.N., Schier, A.F., Engert, F., and Portugues, R. (2012). Brain-wide neuronal dynamics during motor adaptation in zebrafish. Nature *485*, 471–477.

Please cite this article in press as: Odstrcil et al., Functional and ultrastructural analysis of reafferent mechanosensation in larval zebrafish, Current Biology (2021), https://doi.org/10.1016/j.cub.2021.11.007

STAR★METHODS

KEY RESOURCES TABLE

REAGENT or RESOURCE	SOURCE	IDENTIFIER
Antibodies		
Goat anti-Choline Acetyltransferase	Sigma-Aldrich	AB144P
Donkey Anti-Goat IgG H&L (Alexa Fluor 647)	Abcam	ab150135
Chemicals, peptides, and recombinant proteins		
Dextran, Texas Red, 3000 MW	Invitrogen	D3329
Dextran, Alexa Fluor 647, 10,000 MW	Invitrogen	D22914
Dextran, Cascade Blue, 3000 MW	Invitrogen	D7132
Copper(II) sulfate	Sigma-Aldrich	C1297
DiASP: 4-(4-Diethylaminostyryl)-1-methylpyridinium iodide	Sigma-Aldrich	D3418
Cas9 Nuclease	NEB	M0386S
Experimental models: Organisms/strains		
Danio rerio: Tg(elavl3:GCaMP6s)	Chen et al.,[44] Kim et al.[74]	ZFIN: ZDB-ALT-180502-2
Danio rerio: Tg(elavl3:GCaMP6f)	Chen et al.[44]	ZFIN: ZDB-FISH-160927-3
Danio rerio: Tg(Isl1:GFP)	Higashijima et al.[75]	ZFIN: ZDB-FISH-150901-21995
Danio rerio: ETvmat2:GFP	Wen et al.[76]	ZFIN: ZDB-FISH-150901-14862
Danio rerio: Tg(DAT:GFP)	Xi et al.[39]	ZFIN: ZDB-ALT-111206-10
Danio rerio: Tg(Brn3c:GFP)	Xiao et al.[77]	ZFIN: ZDB-ALT-050728-2
Danio rerio: Tg(HGn39D:GFP)	Faucherre et al.[50]	ZFIN: ZDB-FISH-150901-6689
Danio rerio: Tg(elavl3:H2B-mCherry)	Randlett et al.[78]	N/A
Danio rerio: Chrna9aΔ1049	This paper	N/A
Oligonucleotides		
chrna9a_target1: GGACCCCCAGACACTAATGTGG	This paper	N/A
chrna9a_target2: AGAACTCTTGGTGATGGCAGGGG	This paper	N/A
chrna9a_target3: TGCATTCCTGACTATCAAAGGGG	This paper	N/A
chrna9a_target4: CGTACACAGTCCTGCTCAAGCGG	This paper	N/A
chrna9a_target5: GTGGAGCCAAGAAAGAGATGAGG	This paper	N/A
chrna9a_target6: GGGGAGAAGGTCTCGTTGGGGG	This paper	N/A
chrna9a_flanking_PCR_F: GCTCAGTGCAGATGAGGAGG	This paper	N/A
chrna9a_flanking_PCR_R: ACCATCAGCTGAAATACAGTCAGAG	This paper	N/A
Recombinant DNA		
pCS2:lyn-mCherry	Engert Lab	N/A
pCS2:lyn-tdTomato	Engert Lab	N/A
Software and algorithms		
MATLAB	This paper	https://github.com/irisods/ReafferentMechanosensation
LabVIEW	National Instruments	https://www.ni.com/en-us/shop/labview.html
ImageJ	N/A	https://imagej.nih.gov/ij/
VAST	Wee et al.[79]	http://lichtman.rc.fas.harvard.edu/vast
CHOPCHOP v2	Labun et al.[80]	http://chopchop.cbu.uib.no/

RESOURCE AVAILABILITY

Lead contact

Further information and requests for resources and reagents should be directed to and will be fulfilled by the lead contact, Florian Engert (florian@mcb.harvard.edu).

Please cite this article in press as: Odstrcil et al., Functional and ultrastructural analysis of reafferent mechanosensation in larval zebrafish, Current Biology (2021), https://doi.org/10.1016/j.cub.2021.11.007

Materials availability

The *chrna9a* mutant transgenic line generated in this study is available upon request to the lead contact.

Data and code availability

Data analysis code is available at https://github.com/irisods/ReafferentMechanosensation. Due to their large size, datasets are available from the lead contact upon request.

EXPERIMENTAL MODEL AND SUBJECT DETAILS

Zebrafish

We used larval zebrafish (*Danio rerio*) between 4-9 days-post-fertilization (dpf) for all experiments. Transgenic lines include: homozygous Tg(elavl3:GCaMP6s)[74] or Tg(elavl3:GCaMP6f)[44] for functional imaging experiments, Tg(Isl1:GFP)[75] to visualize OEN neurons, ETvmat2:GFP[76] and Tg(DAT:GFP)[39] to label DELL neurons, Tg(Brn3c:GFP)[77] to tag hair cells of the lateral line and inner ear, Tg(HGn39D:GFP)[50] to mark lateral line primary sensory neurons, and Tg(elavl3:H2B-RFP)[78] to label neuronal nuclei. In most cases, animals were also $mitfa^{w2/w2}$ homozygous for their lack of skin-pigmentation.[81] Fish were raised in facility water on a 14/ 10 h light/ dark cycle at 28°C, and fed paramecia daily from 5 dpf. Animal handling and experimental procedures were approved by the Harvard University Standing Committee on the Use of Animals in Research and Training.

METHOD DETAILS

Dye labeling of efferent neurons

Larvae were anesthetized with 0.005% MS-222 (Sigma-Aldrich) and embedded in low melting-point agarose on their sides. Sharpened tungsten needles were used to lesion the lateral line nerve at the level of neuromast L1 and to deposit labeled dextran crystals (Texas Red, Alexa Fluor 647, or Cascade Blue, Invitrogen). Fish were unembedded and allowed to recover for at least 24 h before proceeding with further experimentation.

Capture-recapture random sampling

Neurons were tagged using the dye labeling technique described above. The 'capture' step involved injecting Cascade Blue-conjugated dextrans (3,000 MW, Invitrogen) at the level of the L1 neuromast, at 5 dpf. 48 h were allowed for nerve regeneration.[64] In the 'recapture' step, the injection was repeated in the same location with Alexa Fluor 647-conjugated dextrans (10,000 MW, Invitrogen). The number of neurons labeled with the blue, far red and with both fluorophores were tallied 24 h later and used to calculate the total population size using Chapman's estimator:[82]

$N = \frac{(m2+1)(m1+1)}{o+1} - 1$, where N = total population size, m1 = number of neurons marked the first time, m2 = number of neurons marked the second time and o = number of neurons marked both times (overlap). Chapman's estimator was favored over Lincoln-Petersen's to account for small population sizes and allow for cases where no neurons were marked in both colors. This approach assumes that the population is closed: that no neurons are born or die between labeling sessions. It also assumes that the probability of being 'recaptured' is not influenced by being 'captured' the first time. We performed these experiments on double transgenic animals Tg(elavl3:H2B-RFP) expressing pan-neuronal, nuclear-targeted RFP to aid in counting neurons, and Tg(Isl1:GFP) for anatomical landmarks to distinguish the three hindbrain subnuclei.

Immunohistochemistry

24 h following dye labeling of the lateral line, fish were fixed in 4% paraformaldehyde (PFA) diluted in PBS containing 0.25% Triton (PBT). They were then immunostained using standard procedures.[83] Briefly, fish were washed in PBT, incubated in 150 mM Tris-HCl, pH 9, for 15 min at 70°C, washed in PBT, permeabilized in 1% Proteinase-K during 30 min, washed in PBT, blocked in blocking solution of PBT containing, 2% normal donkey serum (NDS), 1% bovine serum albumin (BSA), 1% dimethyl sulfoxide (DMSO) and then incubated overnight at 4°C in primary antibodies diluted in blocking solution (goat anti-ChAT, 1:200, Sigma-Aldrich). Fish were then washed in PBT, blocked for 1 h and incubated overnight at 4°C in secondary antibodies conjugated to Alexa-647 (donkey anti-goat, 1:1000, Abcam).

Confocal imaging

Imaging of live or fixed tissue after electroporation or immunohistochemistry, respectively, was performed with an upright confocal microscope (Zeiss LSM780) containing a 20x/1.0-NA water-dipping objective.

Focal electroporations

Focal electroporations were performed in double transgenic larvae encoding GFP in hair cells Tg(Brn3c:GFP), and in efferent nuclei by means of Tg(Isl1:GFP) or ETvmat2:GFP to target the OEN or DELL, respectively. Electroporations were performed as described in Tawk et al.[84] Briefly, larvae were anesthetized and embedded in low melting-point agarose dorsal-side up. Micropipettes with tip diameters of 1-2 μm were filled with a 1 μL solution of plasmid DNA in distilled water. pCS2 expression vectors encoding mCherry or tdTomato fused to the N-terminal motif of the Src-family kinase Lyn were used. Guided by GFP expression in landmark areas,

Please cite this article in press as: Odstrcil et al., Functional and ultrastructural analysis of reafferent mechanosensation in larval zebrafish, Current Biology (2021), https://doi.org/10.1016/j.cub.2021.11.007

micropipettes were placed near the efferent nuclei, which were visualized under epi-fluorescence on a compound microscope. A Grass stimulator (SD9, Grass Technologies) was used to deliver plasmids by means of 1-2 200 Hz voltage pulse trains lasting 250 ms in 1 s intervals. Pulses were 20 V in amplitude and 2 ms in duration. Following electroporation, larvae were allowed to recover overnight in fish facility water. The next day, larvae were screened and those containing labeled neurons were anesthetized and mounted in agarose to be imaged using a confocal microscope (Zeiss LSM780).

In vivo 2-photon functional imaging

A custom built 2-photon microscope was used for all functional experiments. The laser, a Ti:Sapphire ultra-fast laser (MaiTai, Spectra-Physics), was tuned to 950 nm, and operated at an average laser power of 5-10 mW at sample. Images were collected by scanning frames at 4 Hz and consecutive planes were separated by 2 μm. Image acquisition was controlled using custom software written in LabView (National Instruments). For experiments involving efferent nuclei, we labeled the lateral line of GCaMP-expressing animals using Texas Red-conjugated dextrans to conclusively identify the neurons. Labeling occurred between 72 and 48 h before functional imaging experiments.

Behavioral tracking during functional imaging

Larvae were embedded in 2% low melting-point agarose in a 35 mm Petri dish one day before imaging. Once the agarose solidified, filtered facility water was added and the agarose around the tail was removed with a scalpel to allow for free movement of the tail. To image, the dish was placed on the microscope's transparent stage, which was covered with a diffusive screen onto which visual stimuli were projected. The screen also had a small hole to make the fish's tail visible and recordable from below. Animals were illuminated with infrared light-emitting diodes (wavelength: 850 nm) and recorded at 200 frames per second (100 for heat experiments) using an infrared-sensitive camera (Pike F032B, Allied Vision Technologies). The cumulative angle of the tail was computed online and recorded as in Portugues and Engert[85] to determine the start and ends of individual swim bouts. This was used to update visual feedback in experiments with optomotor gratings and for analysis of locomotion throughout this study. Acquisition and stimulus presentation were controlled by custom LabView (National Instruments) programs.

Stimulus delivery during functional imaging

Optomotor gratings: visual stimuli were projected onto the screen under the fish at 60 frames per second using a 3M MPro110 microprojector fitted with a red long-pass filter (Kodak Wratten Nr. 25) to enable imaging and visual stimulation simultaneously.[85] The stimulus consisted of a square wave grating with a spatial period of 10 mm and 100% contrast (darkest and lightest pixels possible). Per imaging plane, the grating alternated 6 times every 20 s between being static or moving at 10 mm/s in the caudo-rostral direction. If a swim bout was detected, the grating speed was adjusted online to deliver the appropriate visual feedback in a closed-loop fashion.

Flow

A custom-built syringe pump system was used to deliver filtered fish facility water through a zero-dead-volume perfusion pencil (AutoMate Scientific), which was placed near the head of the fish as in Wee et al.[79] After 4 s of baseline, 500 μl of fish facility water was delivered for 3.3 s. This was repeated every 20 s, 4 times per imaging plane.

Taps

A solenoid was fixed to the microscope stage and triggered by voltage pulses.[58] The strength of the pulse was empirically determined for each fish at the beginning of an experiment to ensure that the animals would not respond to every tap. 4 taps were delivered per imagining plane, with interstimulus intervals of 10 or 15 s to avoid habituation.

Heat

Heat stimuli were delivered as in Haesemeyer et al.[86] A 1 W 980 nm fiber-coupled diode laser (Roithner, Austria) coupled into a collimator (Aistana, USA) was placed under the objective pointing downward at the fish at an angle of 16.5°, at a distance of 4 mm in front and 1.2 mm above. Laser power was programmatically controlled via a laser diode driver (Thorlabs, USA). Heat was delivered for 2 s in 20 s blocks (9 s off, 2 s on, 9 s off), 10 times in each imaging plane. The laser power at sample was 350 mW, heating the larva to a temperature of ~30°C, which is aversive but below the noxious threshold.

Chemical ablation of neuromasts

Fish were incubated in 1 mM copper sulfate for 85 min and allowed to recover in fish facility water for 60 min. Only animals showing complete neuromast ablation (assessed by DiASP staining: 0.5 mM in fish facility water for 15 min, as in Schuster and Ghysen[87]) were used for functional imaging.

Tissue preparation for ssSEM

A double transgenic zebrafish larva (Isl1:GFP and DAT:tdTomato) was used to visualize the two efferent nuclei with different fluorescent markers. At 5 dpf, the animal was anaesthetized in fish facility water containing 0.02% (w/v) tricaine mesylate (MS-222, Sigma-Aldrich), and embedded in 2% low melting-point agarose, lateral side up. The posterior lateral line neuromast (L1) was imaged under a confocal microscope to capture the pattern of innervation of the fluorescently-labeled efferent axons. L1 was selected because it lies above the swim bladder, which can be used as a landmark for subsequent steps. The animal was then prepared for fixation. Both eyes were enucleated in a dissection solution containing 0.02% (w/v) tricaine mesylate,[88] and the body was immediately transferred into cold fixative solution (2.5% glutaraldehyde, 2% paraformaldehyde, 3.5% mannitol, 0.15 M sodium cacodylate buffer) and

underwent two microwave fixation rounds[73] followed by overnight incubation at 4°C. Fixation continued for an additional 8 h with 2.5% glutaraldehyde, 3.5% mannitol, 0.15 M sodium cacodylate buffer and wash (0.15 M sodium cacodylate, 3x10 min). The sample was reduced with 0.8%(w/v) sodium hydrosulfite in 60% (v/v) 0.1 M sodium bicarbonate 40% (v/v) 0.1 sodium carbonate buffer with 3 mM CaCl2 for 20 min and washed with buffer (3x10 min). Heavy metal staining was achieved as follows: 2% osmium, 0.15 M sodium cacodylate (4 h RT, 4°C overnight), 2.5% (w/v) potassium ferrocyanide in 0.15 M sodium cacodylate (4 h RT, 4°C overnight), wash with ddH2O water (3x10 min), filtered 1% (w/v) thiocarbohydrazide (TCH) in ddH2O (1 h, RT), wash with ddH2O and overnight incubation with 1% uranyl acetate (UA) at 4°C. The animal was then freed from the agarose and dehydrated with serial ethanol dilutions (25%, 50%, 75%, 90%, 100%, 100% ethanol in water, 10 min each) and 100% propylene oxide (PPO, 2x10 min). The sample was infiltrated with a series dilution of LX-112 resin and PPO (25%, 50%, 75% for 6 h and 100% overnight), embedded at 60°C for 72 h. The cured block was trimmed, mounted, cut in 30 nm thick sections and imaged as in Hildebrand et al.[89]

Volumetric reconstructions from ssEM data

ssEM images were aligned using non-affine alignment through the FijiBento package on the Odyssey cluster supported by the FAS Division of Science, Research Computing Group at Harvard University.[90] Image segmentation was carried out manually using a custom volume annotation and segmentation tool. Segmented images were processed for 3D modeling with MATLAB and 3Ds Max for rendering. VAST: http://lichtman.rc.fas.harvard.edu/vast

Laser ablations of efferent nuclei

Fish were subjected to unilateral dye injections in the lateral line at 4 dpf as described above, and allowed to recover in freely-swimming conditions for 48 h to allow for nerve regeneration after injury.[65] At 6 dpf, fish were embedded in low-point melting agarose, and the agarose surrounding their tails was removed. Functional experiments were performed the following day. After a round of baseline functional experiments, we performed the ablation procedure as described in Orger et al.,[53] with the exception that anesthesia was not used. Individual efferent neurons were targeted systematically with 1-3 850 nm laser pulses of 1 ms, at 80% laser power. Fish were then immediately used for functional experiments to test for the effects of ablations on sensory processing. On average, 4 OEN efferent neurons were ablated from the 8 that are hypothesized to exist (Figure S5B).

Generation of chrna9a mutants using CRISPR–Cas9

Six Cas9 target sites within the *chrna9a* open reading frame were chosen using CHOPCHOP v2[80] to generate single-guide RNAs (sgRNAs) for mutagenesis. DNA templates for transcription of sgRNAs were generated using oligo annealing and fill-in as previously described.[91] Cas9 protein (NEB) was mixed with all six sgRNAs and injected into embryos at the 1-cell stage. Clutches from outcrosses of these injected fish were screened by PCR using flanking primers and sequencing was used to identify a 1049 bp deletion allele that deleted much of the third and fourth exons and generated a frameshift (Figure S5F). Founders were outcrossed repeatedly with Tg(elavl3:GCaMP6s) animals to reduce the likelihood of unlinked, off-target mutations affecting the *chrna9a* null genotype, and to be able to perform functional imaging experiments. Mutant fish were genotyped using a two primer PCR-based strategy. CRISPR target sites and primer sequences are listed below.

chrna9a_target1 GGACCCCCAGACACTAATGTGG
chrna9a_target2 AGAACTCTTGGTGATGGCAGGGG
chrna9a_target3 TGCATTCCTGACTATCAAAGGGG
chrna9a_target4 CGTACACAGTCCTGCTCAAGCGG
chrna9a_target5 GTGGAGCCAAGAAAGAGATGAGG
chrna9a_target6 GGGGAGAAGGTCTCGTTGGGGG
chrna9a_flanking_PCR_F GCTCAGTGCAGATGAGGAGG
chrna9a_flanking_PCR_R ACCATCAGCTGAAATACAGTCAGAG

QUANTIFICATION AND STATISTICAL ANALYSIS

Data analysis

Data analysis was performed using scripts written in MATLAB (MathWorks).

Images were segmented manually to define ROIs corresponding to individual neurons using VAST.[92] Segmentation was performed on an 'anatomical stack' obtained by computing the mean of the time-series for each plane. OEN and DELL neurons were identified by lateral line dye labeling, and segmentation was therefore performed on anatomical stacks obtained from the Alexa Fluor 647 signal in the volume imaged during the functional recordings. The PLLg can be clearly identified in GCaMP expressing animals as a ganglion posterior to the ear, so afferent neurons were segmented from anatomical stacks arising from the calcium imaging data.

The time-series of the fluorescence signal F(t) for each neuron was computed as the mean intensity of all pixels comprising an ROI in each imaging frame. The proportional change in fluorescence (ΔF/F) at time t was calculated as: $\Delta F/F = \frac{F(t)-F0}{F0}$, where F0 for any

Please cite this article in press as: Odstrcil et al., Functional and ultrastructural analysis of reafferent mechanosensation in larval zebrafish, Current Biology (2021), https://doi.org/10.1016/j.cub.2021.11.007

ROI is the 20th percentile of its entire fluorescence signal per plane. Perceptually uniform color maps developed by Ander Biguri were used to graph the average single-cell responses in Figure 2. https://www.mathworks.com/matlabcentral/fileexchange/51986-perceptually-uniform-colormaps

To compute swim-triggered averages and for analyses correlating neuronal activity to different features of swim kinematics (Figures 3M–3O, S3G, S3H, and S3Q–S), only 'unitary' bouts were taken into account. That is, bouts that occurred after at least 4 s from a previous bout and that were not followed by a subsequent bout within 2.5 s. The selected swim features were (1) Swim power, defined as the integral of the absolute tail curvature trace for an individual bout, as in Ahrens et al.[93] (2) Maximum amplitude, the maximum tail curvature achieved per bout and (3) Tail beat frequency, the inverse of the time between successive extreme tail positions in the same direction, as in Severi et al.[54] Neuronal activity was defined as the integral of the calcium transient during each corresponding bout. Pearson's coefficients correlating each bout feature with neuronal activity were calculated for each efferent neuron.

In order to quantify the change in PLLg activity after the ablation of efferent nuclei, and be able to compare effects across fish, the $\Delta F/F$ trace for each PLLg neuron was z-scored, and the average neuronal activity 4 s after a swim was subtracted to the average activity 4 s before a swim. A result of 0 indicates no difference in neuronal activity during swims or quiescent periods, whereas a positive result would indicate motor-correlated neuronal activity. Normalized differences were computed for each cell before and after ablations. Finally, the median of the normalized differences of all cells in a ganglion was calculated and used as the representative statistic for each animal (Figures 5C and 5F). A similar approach was taken when comparing PLLg activity in *chrna9a* mutants versus wildtypes (Figure 5I). In this case, the entire PLLg was considered a single ROI instead of individually segmenting its neurons.

Statistical analysis

All swim- and stimulus-triggered average plots show the mean ± SEM across fish. Significance was determined using nonparametric statistical tests: the Wilcoxon signed-rank test for paired data, and the Wilcoxon rank-sum test for independent samples. Two-tailed p values are reported for all tests as follows: * $p \leq 0.05$ and ** $p \leq 0.001$. For correlation analysis, Pearson's correlation was computed. When comparing fish populations of multiple genotypes (Figure 5I), the nonparametric Kruskal-Wallis one-way analysis of variance (ANOVA) test was used, followed by Bonferroni corrected unpaired Wilcoxon rank-sum tests. In these cases, the genotype was determined post hoc and disclosed after the functional data had been analyzed. No statistical methods were used to predetermine sample size.

Current Biology, Volume *32*

Supplemental Information

Functional and ultrastructural analysis of reafferent mechanosensation in larval zebrafish

Iris Odstrcil, Mariela D. Petkova, Martin Haesemeyer, Jonathan Boulanger-Weill, Maxim Nikitchenko, James A. Gagnon, Pablo Oteiza, Richard Schalek, Adi Peleg, Ruben Portugues, Jeff W. Lichtman, and Florian Engert

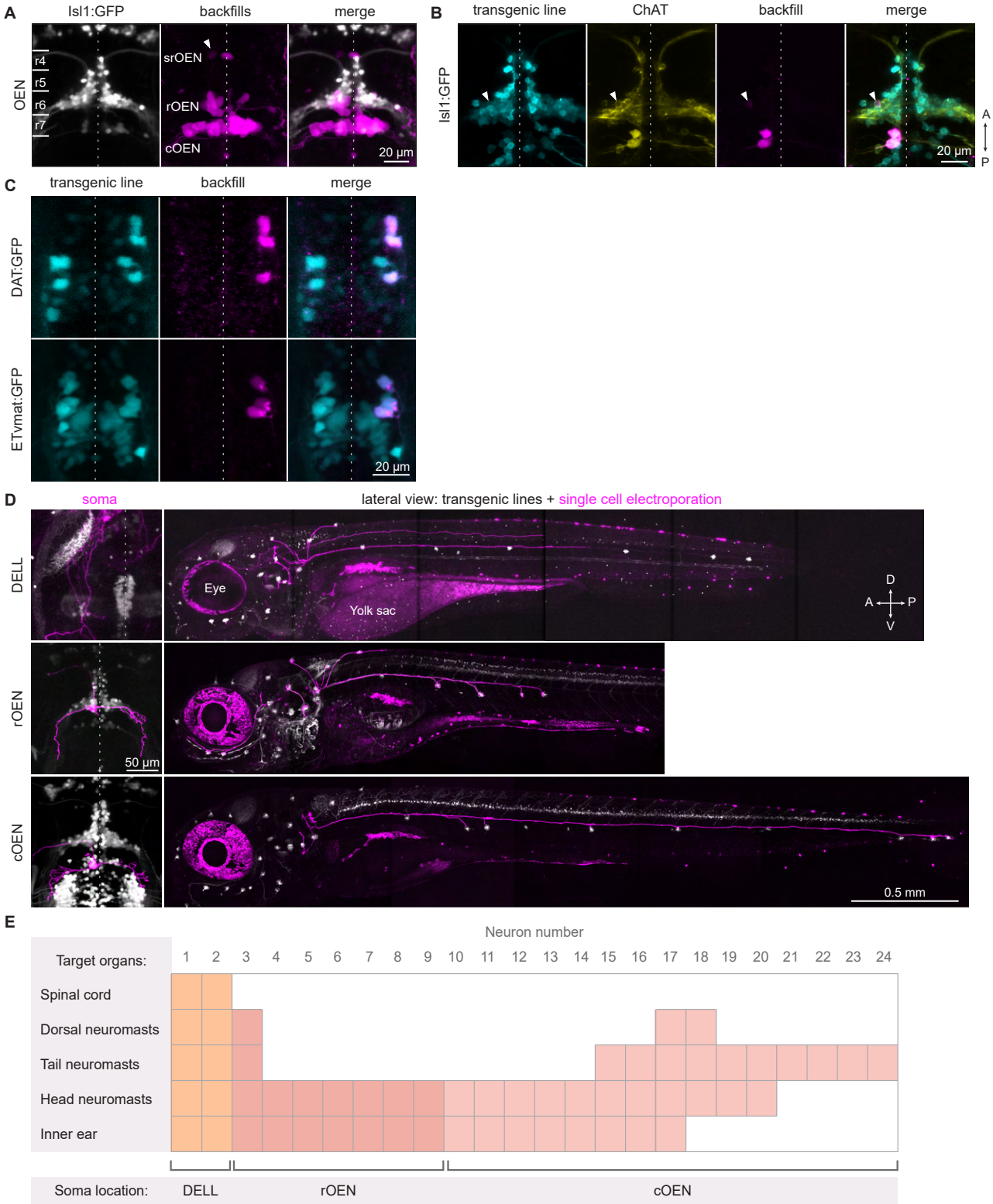
A
Isl1:GFP
backfills
merge
OEN
r4
r5
r6
r7
srOEN
rOEN
cOEN
20 µm
B
transgenic line
ChAT
backfill
merge
Isl1:GFP
A
P
20 µm
C
transgenic line
backfill
merge
DAT:GFP
ETvmat:GFP
20 µm
D
soma
lateral view: transgenic lines + single cell electroporation
DELL
Eye
Yolk sac
D
A
P
V
rOEN
50 µm
cOEN
0.5 mm
E
Neuron number
Target organs:
1 2 3 4 5 6 7 8 9 10 11 12 13 14 15 16 17 18 19 20 21 22 23 24
Spinal cord
Dorsal neuromasts
Tail neuromasts
Head neuromasts
Inner ear
Soma location:
DELL
rOEN
cOEN

Figure S1. Characterization of neurotransmitter identity and target of efferent nuclei. Related to Figure 1.
(A) Composite image showing all hindbrain neurons labeled after dye injections of the lateral line nerve in Isl1:GFP larvae. Images were registered using anatomical landmarks made visible by GFP expression. The labeled neurons occupy three distinct positions along the antero-posterior axis spanning rhombomeres r4 to r7, and are named accordingly: caudal, rostral, and supra-rostral OEN (n=17 fish, 6 bilateral). Dotted line: midline. Arrowhead: srOEN neuron. **(B)** Maximum intensity projections of confocal images of an Isl1:GFP larval hindbrain after a unilateral lateral line nerve dye injection and subsequent antibody stain against choline acetyltransferase (ChAT). Arrowhead: labeled neuron in the rOEN. **(C)** Maximum intensity projections of confocal images of the hypothalamus of transgenic larvae following unilateral lateral line nerve dye injections. Neurons labeled by the injections also express GFP under the Dopamine Active Transporter (DAT, top), and the Vesicular Monoamine Transporter (VMAT, bottom) promoters. **(D)** Focal electroporations of membrane-tagged fluorescent proteins reveal efferent neuron morphologies. Maximum intensity projections of confocal images showing the morphology of single lateral line efferent neurons. Dorsal and lateral views of single cells (magenta) electroporated in double transgenic larvae expressing GFP in all hair cells, Tg(Brn3c:GFP), and in additional lines that label the efferent nuclei (gray). Top: DELL neurons in the ETvmat2:GFP background (5 dpf). Middle/bottom: rostral and caudal OEN neurons in Isl1:GFP fish (10 and 8 dpf, respectively). We were unable to successfully label a single srOEN neuron using this technique. Note: both the eyes and the yolk sac are auto-fluorescent and therefore also appear magenta. This signal is unrelated to the electroporations. **(E)** Matrix summarizing the observed target organs of individual efferent neurons, which were made visible using single cell electroporations (n= 24 fish, one neuron per fish).

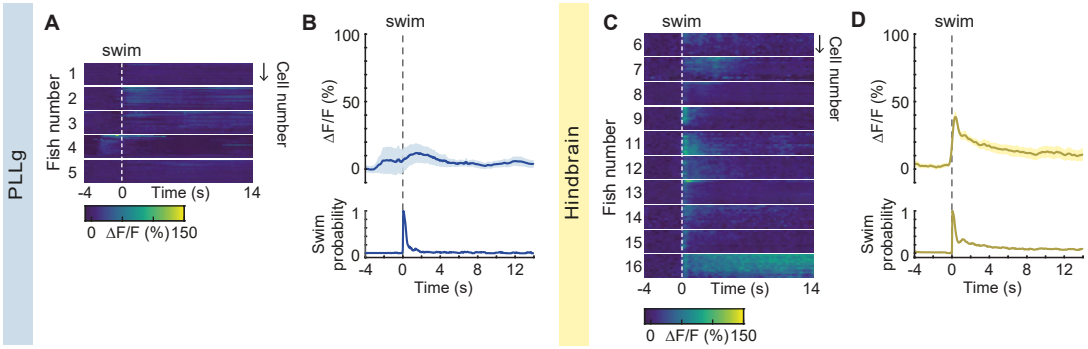

Figure S2. Activity of PLLg primary sensory neurons and hindbrain neurons during head-restrained swimming. Related to Figure 2.

(A) Average single-cell responses (ΔF/F) during spontaneous swim bouts of neurons belonging to the corresponding 5 flow-sensitive fish in Figure 2C (n= 20, 26, 16, 24, 30 cells). **(B)** Population swim-triggered averages of neuronal activity in the PLLg (mean ΔF/F ± s.e.m.). Bottom: swim probability during the same period. Averages arise from the single-cell measurements shown in Figure S2A. **(C)** Average single-cell responses (ΔF/F) of hindbrain neurons in the vicinity of the PLLg belonging to the corresponding fish in Figure 2F (n= 11 cells per fish). Note that fish 10 is missing since no hindbrain neurons were imaged in this fish. Fish 16 showed strong and prolonged hindbrain activity reflecting sustained OMR-induced swim activity. **(D)** Population swim-triggered averages of neuronal activity in hindbrain neurons (mean Δ F/F ± s.e.m.). Bottom: swim probability during the same period. Averages arise from the single-cell measurements shown in Figure S2C.

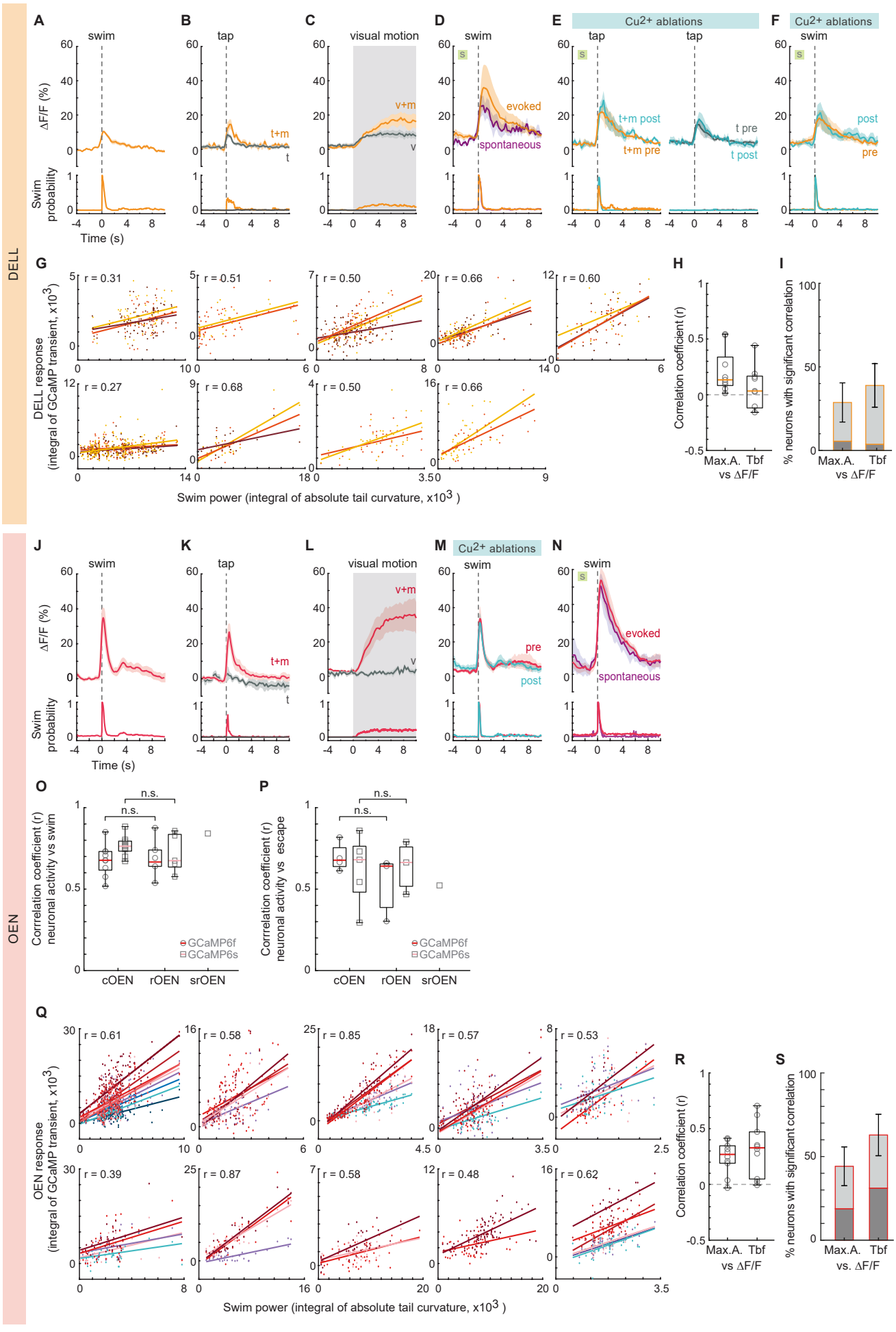
DELL
OEN
A
B
C
D
E
F
G
H
I
J
K
L
M
N
O
P
Q
R
S
swim
tap
visual motion
Cu2+ ablations
ΔF/F (%)
Swim probability
Time (s)
t+m
t
v+m
v
evoked
spontaneous
t+m post
t+m pre
t pre
t post
post
pre
DELL response (integral of GCaMP transient, x10^3)
OEN response (integral of GCaMP transient, x10^3)
Swim power (integral of absolute tail curvature, x10^3)
Correlation coefficient (r)
% neurons with significant correlation
Max.A. vs ΔF/F
Tbf vs ΔF/F
Corrrelation coefficient (r) neuronal activity vs swim
Corrrelation coefficient (r) neuronal activity vs escape
GCaMP6f
GCaMP6s
cOEN
rOEN
srOEN
n.s.

Figure S3. Activity of efferent nuclei during locomotion and in response to diverse sensory stimuli. Related to Figure 3.

Most experiments were performed on fish expressing GCaMP6f. Instances using GCaMP6s animals are signaled by an 'S' on a green square. **(A-F)** Top: Population averages of DELL neuronal activity (mean ΔF/F ± s.e.m.). Bottom: swim probability. **(A)** Average swim-triggered neuronal responses (n= 6 fish). **(B)** Average stimulus-triggered neuronal responses to taps that elicited motor responses (t+m, orange) and taps that did not (t, gray) (n= 5 fish). **(C)** Average stimulus-triggered responses during periods of moving visual gratings that elicited (v+m, orange) and failed to elicit (v, gray) motor responses (n= 8 fish). **(D)** Average swim-triggered neuronal responses after swim bouts that were spontaneous (purple) or evoked by a moving grating (orange) (n= 5 fish). **(E)** Average stimulus-triggered neuronal responses to taps before and after ablation of the lateral line using copper sulfate. Responses are separated depending on whether the tap elicited (left) or did not elicit (right) motor responses (n= 4 fish). **(F)** Average swim-triggered neuronal responses before and after ablation of the lateral line by copper sulfate (n= 6 fish). **(G)** Scatter plots showing the relationship between the power of each individual swim bout versus the intensity of the concurrent neuronal responses of all labeled DELL neurons in each of the 9 fish analyzed. Correlation coefficients and best-fit lines arising from linear regression were calculated for each neuron (shown in different shades), and used to calculate the mean correlation coefficient (r) per fish. Swim power was defined as the integral of the absolute tail curvature trace for individual bouts: a stationary tail has little curvature and thus power is ~0, whereas an undulating tail has a positive absolute tail curvature, which increases as a function of motor strength. Neuronal activity was defined as the integral of the calcium transient during each corresponding bout. **(H)** Box plots showing the mean Pearson's coefficients correlating maximum tail amplitude (Max. A.) or tail beat frequency (Tbf) of single bouts with the concurrent neuronal activity of DELL neurons in individual fish (gray circles, n= 9 fish). Median shown in color. **(I)** Mean percentage of DELL cells per fish whose activity was significantly correlated with maximum tail amplitude or tail beat frequency (n= 9 fish, dark gray $p < 0.001$, light gray < 0.05, error bars: s.e.m). **(J-N)** Top: Population averages of OEN neuronal activity (mean ΔF/F ± s.e.m.). Bottom: swim probability. **(J)** Average swim-triggered neuronal responses (n= 9 fish). **(K)** Average stimulus-triggered neuronal responses to taps that elicited motor responses (t+m, red) and taps that did not (t, gray) (n= 5 fish). **(L)** Average stimulus-triggered responses during periods of moving visual gratings that elicited (v+m, red) and failed to elicit (v, gray) motor responses (n= 10 fish). **(M)** Average swim-triggered neuronal responses before and after ablation of the lateral line by copper sulfate (n= 6 fish). **(N)** Average swim-triggered neuronal responses after swim bouts that were spontaneous (purple) or evoked by a moving grating (red) (n= 7 fish). **(O)** Boxplots of mean Pearson's coefficients relating swimming behavior and neuronal activity (ΔF/F) in different OEN subnuclei of fish expressing GCaMP6f (circles, c=9, r=6) or 6s (squares, c=8, r=5, sr=1). Medians shown in color. Locomotor behavior was convolved with a calcium kernel to account for calcium dynamics. (Pearson's correlation, $p<0.001$; 2-tailed Wilcoxon rank-sum test, p= 0.86 and 0.52 for GCaMP6f and 6s, respectively.) **(P)** Boxplots of mean population Pearson's coefficients relating short-latency escape behaviors and neuronal activity (ΔF/F) in different OEN subnuclei of fish expressing GCaMP6f (circles, c=5, m=3) or 6s (squares, c=5, r=3, sr=1). Median shown in color. Locomotor behavior was convolved with a calcium kernel to account for calcium dynamics. (Pearson's correlation, $p<0.001$; 2-tailed Wilcoxon rank-sum test, p= 0.23 and 0.99 for GCaMP6f and 6s, respectively.) **(Q)** Scatter plots showing the relationship between the power of all individual swim bouts versus the neuronal responses of all labeled OEN neurons in each of the 10 fish analyzed. Correlation coefficients and best-fit lines arising from linear regression were calculated for each neuron (shown in different shades), and used to calculate the mean correlation coefficient (r) per fish. **(R)** Box plots of mean Pearson's coefficients correlating maximum tail amplitude (Max.A.) or tail beat frequency (Tbf) of single bouts with the concurrent neuronal activity of OEN neurons of individual fish (gray squares, n= 10 fish). Median shown in color. **(S)** Mean percentage of OEN cells per fish whose activity was significantly correlated with maximum tail amplitude or tail beat frequency (n= 10 fish, dark gray $p < 0.001$, light gray < 0.05, error bars: s.e.m).

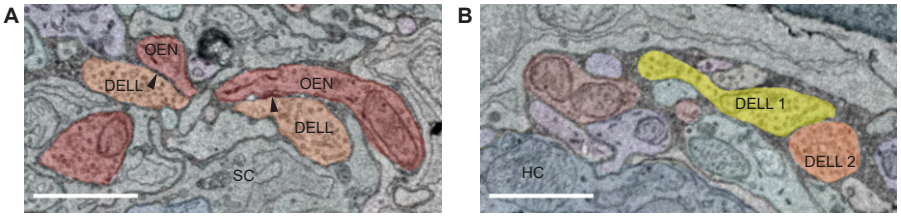

Figure S4. ssEM images of efferent to efferent connections in a posterior lateral line neuromast. Related to Figure 4.
(A) DELL vesicle-filled profiles in close apposition to an OEN axon (arrowheads), surrounded by a support cell (SC).
(B) Vesicle-filled profiles from two separate DELL neurons contact each other. A hair cell (HC) is also labeled for reference. Scale bars: 1 μm.

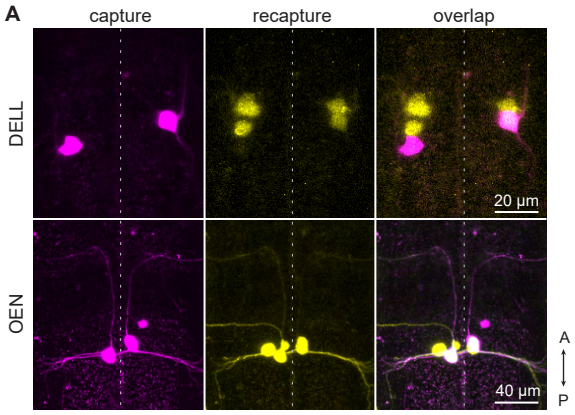

B

Efferent nucleus	Population estimate (unilateral)	Maximum labeled	n
DELL	3.02 ± 1.13	5	48
srOEN	1.00 ± 0.00	1	2
rOEN	1.86 ± 0.84	3	25
cOEN	2.66 ± 1.25	5	43

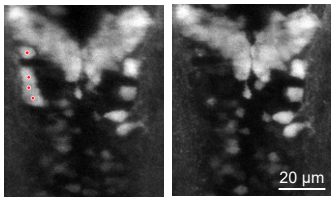

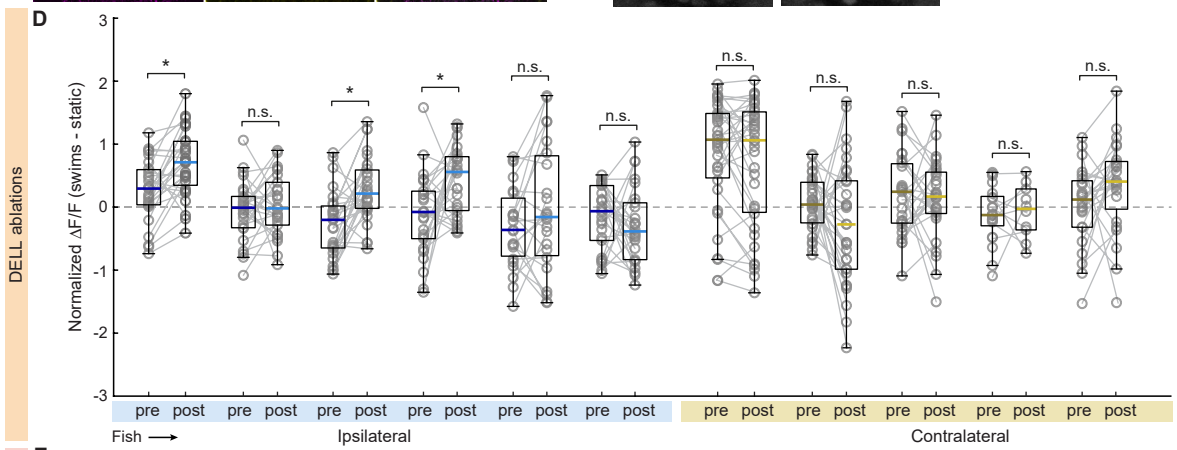

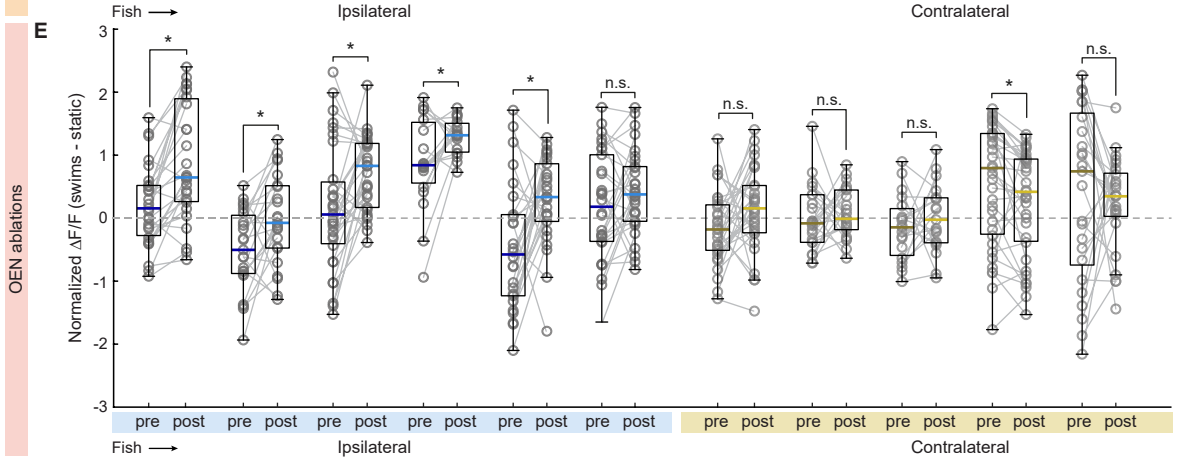

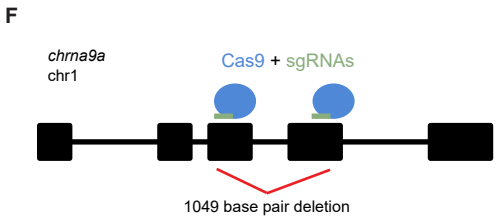

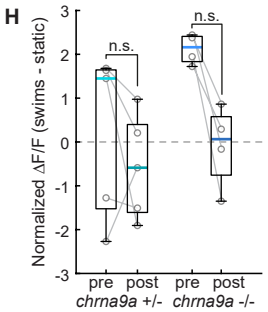

G

```
chrna9a       MEGYSNALRPVEDTDKALNVTLQITLSQIKDMDERNQVLTTYLWVRQIWHDAYLSWDKEEYDGLEVIRIPSNLVWRPDIVLYNNADEEDSSGPPDTNVVLRYNGEITWDSPAITKSSCKV
chrna9Δ1049   MEGYSNALRPVEDTDKALNVTLQITLSQIKDMDERNQVLTTYLWVRQIWHDAYLSWDKEEYDGLEVIRIPSNLVWRPDIVLYNNADEEDSSGPPDTGYGPAGSDCISADGS--------

chrna9a       DVSYFPFDSQECNLTFGSWTYNGNQVDIAMGMESGDLSDFVDNVEWECHGMPAVKNVIMYGCCSDPYPDITYTVLLKRRSSFYIFNLLLPCFLISFLAPLGFYLPADSGEKVSLGVTVLL
chrna9aΔ1049  ----------------------------------------------------------------------------------------------------------------------------

chrna9a       ALTVFQLMVAESMPPSESVPLIGKYYIATMTMITASTSLTIFIMNIHFCGAEAKPVPHWAKVLIIDYMSKIFFVYEVGENCTTPESDRGPFFSEDPLASLERDGYFDKGFYEDCHLDERI
chrna9aΔ1049  ----------------------------------------------------------------------------------------------------------------------------

chrna9a       RSQFNGYSHRDHRHGNGYHHKNSSYRQHRNEQQRRTRSSSNSPVRQSSHHPKYTHFIGRDGSEKLPLTSQEKLKDSEISIPEKINGYTYDQGNGYLNGVGYLHDNGYSKTFGADSYNKTT
chrna9aΔ1049  ----------------------------------------------------------------------------------------------------------------------------

chrna9a       TGTGCVCGKHQKLVRNIEYIANCFREQRGHQAKGAEWKKVAKVMDRFFMWVFFIMVFLMSILVLAKAT
chrna9aΔ1049  ------------------------------------------------------------------
```

Figure S5. Efferent nuclei size estimation, effects of efferent nuclei laser ablation on PLLg activity and generation of mutants lacking α9-nAChRs. Related to Figure 5.

(A) Dorsal projections of confocal images of fish that underwent consecutive dye injections of the lateral line nerve to estimate efferent population size. Top: DELL neurons, bottom: OEN neurons. **(B)** Estimated number of neurons comprising each efferent nucleus innervating the PLL. **(C)** Dorsal projections of confocal images of DELL neurons before and after laser ablations. Red dots indicate targeted neurons. **(D-E)** Boxplots of z-scored ΔF/F showing the difference in activity during swimming and quiescent periods of single neurons in PLL ganglia located ipsilaterally (blue) or contralaterally (yellow) to the ablation site. Medians shown in color. **(D)** Differences were computed for each neuron before and after DELL ablations. Paired 2-tailed Wilcoxon signed-rank test: $p_{ipsilateral}$= 0.3257,0.0714, 0.8854, 0.9219, 0.0814, $p_{contralateral}$= 0.0014, 0.3673, 0.0014, 0.0107, 0.2238, 0.3158. **(E)** Differences were computed for each neuron before and after OEN ablations. Paired 2-tailed Wilcoxon signed-rank test: $p_{ipsilateral}$= $9.994x10^{-4}$, 0.0089, 0.0057, 0.0269, 0.0107, 0.1714, $p_{contralateral}$= 0.0524, 0.6378, 0.3547, 0.0032, 0.5449. **(F)** Diagram of the *chrna9a* gene highlighting the CRISPR-Cas9 target sites in exons 3 and 4 and the 1049 base pair region deleted in the mutant. Introns are depicted as thin lines. **(G)** Predicted amino acid sequence of the wild-type Chrna9a and mutant Chrna9aΔ1049 proteins. Shared sequences are highlighted in gray and amino acids changed due to frameshift in red. **(H)** Boxplots of z-scored population ΔF/F per fish showing the difference in neuronal activity during swimming and quiescent periods in mutant animals before and after lateral line ablation with copper sulfate. Medians shown in color. Paired 2-tailed Wilcoxon signed-rank test: $p_{+/-}$= 0.4375, $p_{-/-}$= 0.1250.